Front. Phys., 2013, 8(6): 630–660
DOI 10.1007/s11467-013-0306-z

REVIEW ARTICLE

Black hole binaries and microquasars

Shuang-Nan Zhang[1,2]

[1] *Laboratory for Particle Astrophysics, Institute of High Energy Physics, Beijing 100049, China*
[2] *National Astronomical Observatories, Chinese Academy of Sciences, Beijing 100012, China*
E-mail: zhangsn@ihep.ac.cn

Received December 7, 2012; accepted February 22, 2013

This is a general review on the observations and physics of black hole X-ray binaries and microquasars, with the emphasize on recent developments in the high energy regime. The focus is put on understanding the accretion flows and measuring the parameters of black holes in them. It includes mainly two parts: i) Brief review of several recent review article on this subject; ii) Further development on several topics, including black hole spin measurements, hot accretion flows, corona formation, state transitions and thermal stability of standard think disk. This is thus not a regular bottom-up approach, which I feel not necessary at this stage. Major effort is made in making and incorporating from many sources useful plots and illustrations, in order to make this article more comprehensible to non-expert readers. In the end I attempt to make a unification scheme on the accretion-outflow (wind/jet) connections of all types of accreting BHs of all accretion rates and all BH mass scales, and finally provide a brief outlook.

Keywords accretion and accretion disks, neutron stars, black holes, jets and bursts, X-ray sources, γ-ray sources, X-ray binaries

PACS numbers 97.10.Gz, 97.60.Jd, 97.60.Lf, 98.58.Fd, 98.62.Nx, 98.70.Qy, 98.70.Rz, 97.80.Jp

Contents

1 Synopsis 630
2 Acronyms and terminology 631
3 Review of reviews 632
3.1 The most recent *Science* collection 632
3.2 The most recent ARA&A article on BHXBs, with some updates 634
3.3 Two comprehensive and long articles on modeling accretion flows in BHXBs 637
3.3.1 A beginner's guide 637
3.3.2 An expert's handbook 639
4 Further developments on BH spin measurements 641
4.1 The first black hole spin measurement with X-ray spectral continuum fitting 643
4.2 Further developments and applications of the continuum fitting method 643
4.3 Uncertainties of the continuum fitting method 646
4.4 Future improvements of the continuum fitting method 647
4.5 Possible application of the continuum fitting method to AGNs 649
5 Further developments on hot accretion flows 650
6 Further developments on corona formation 651
7 Further developments on state transitions 653
8 Further developments on thermal stability of SSD 654
9 Unification and outlook 655
Acknowledgements 657
References 657

1 Synopsis

I will start by defining what I mean by black hole binaries (BHBs) and microquasars in this article. I decide to restrict myself to only a subclass of BHBs, namely, BH X-ray binaries (BHXBs), since these are the only class of BHBs known observationally. I will then simply refer microquasars as BHXBs for reasons discussed in Section 2.

Since many excellent, comprehensive and quite up-to-date review articles on BHXBs are readily available in literature, I feel it is not necessary to write another bottom-up and comprehensive review article on the same subjects at this stage. I will thus take quite an unusual approach in this article. I will first give some concise guides

© Higher Education Press and Springer-Verlag Berlin Heidelberg 2013

Frontiers of Physics

on several representative review articles [1–4], with some necessary updates. I will then focus on the further developments on several topics I feel deserve more discussions, i.e., BH spin measurements (Section 4), hot accretion flows (Section 5), corona formation (Section 5), state transitions (Section 7) and thermal stability of SSD (Section 8). The emphasis is thus put on understanding the accretion flows and measuring the parameters of black holes in them. Some rather general issues on BH astrophysics, such as what astrophysical BHs are and how to identify them observationally, are not discussed here but can be found from my recent book chapter entitled "Astrophysical Black Holes in the Physical Universe" [5].

The usual practice of writing a review article is to end by listing some outstanding issues and major unsolved problems, and then to propose some possible approaches to them. I initially did not do this in the first draft. The history of astronomy tells us that major progress is almost always made by unexpected discoveries and research results; unpredictability is an essential nature of astronomy. This article is not intended to be read by funding agencies or proposal reviewers, so I thought I did not have to do it. In astronomy, knowing what has happened, but looking and doing it differently are far more important and effective than following other people's advises. However, the editors of this book suggested me to write a brief "outlook" in the end. I thus did it nevertheless.

2 Acronyms and terminology

In Table 1, I list all acronyms used in this article; most of these are quite commonly used in this community.

A BH binary (BHB) is a gravitationally bound binary system in which one of the objects is a stellar mass BH with mass from several to tens of solar masses ($M_\odot$); the other object, i.e. its companion, can be either a normal star, a white dwarf, or a neutron star (NS). In case a binary system consists of two BHs, it is is referred to as a binary BH system, which is not covered in this article. When the companion in a BHB is a normal star, the gas from the star may be accreted to the BH and X-rays are produced, as a consequence of the heating by converting the gravitational potential energy into the kinetic energy of the gas, and a *BH X-ray binary* (BHXB) is referred to as such a binary system, as shown in Fig. 1. The possible existence of BHXBs was first suggested by Zel'dovich & Novikov [6, 7]. The first BHXB found is Cygnus X–1 [8], now a well-studied system among many others found subsequently in the Milky Way and nearby galaxies.

The terminology of *microquasar* has some twisting in it. Historically it was first referred to the BHXB 1E1740.7−2942 in the Galactic center region, because a double-sided jet was detected from it, mimicking some quasars with similar radio lobes, which have much larger

Table 1 List of acronyms.

Acronym	Definition
ADAF	advection dominated accretion flow
ADIOS	advection dominated accretion inflow/outflow solution
AGN	active galactic nuclei
BH	black hole
BHB	black hole binary
BHXB	black hole X-ray binary
BL3Q	broad-line-less luminous quasar
BLR	broad-line region
BP	Blandford–Payne
BZ	Blandford–Znajek
CDAF	convection dominated accretion flow
CF	continuum fitting
DIM	disk instability model
FRED	fast rise and exponential decay
FSRQ	flat spectrum radio quasar
GR	general relativity
GRB	gamma-ray burst
HAF	hot accretion flow
HFQPO	high frequency quasi-periodic oscillation
HID	Hardness-Intensity-Diagram
HIF	hot inner flow
ISCO	inner-most stable circular orbit
JDAF	jet dominated accretion flow
LFQPO	low frequency quasi-periodic oscillation
LHAF	luminous hot accretion flow
LLAGN	low-luminosity AGN
LMC	Large Magellanic Cloud
LMXB	low-mass X-ray binary
NDAF	neutrino dominated accretion flow
NS	neutron star
NSXB	neutron star X-ray binary
PDS	power density spectrum
PL	power-law
QPO	quasi-periodic oscillation
RID	RMS-Intensity-Diagram
RMS	root-mean-squares
RQQ	radio-quiet quasar
SEAF	Super-Eddington accretion flow
SLE	Shapiro, Lightman & Eardley
SPL	steep power-law
SSD	Shakura–Sunyaev Disk
SXE	soft X-ray excess
TID	truncated inner disk
ULX	ultra-luminous X-ray source
WD	white dwarf
XRB	X-ray binary

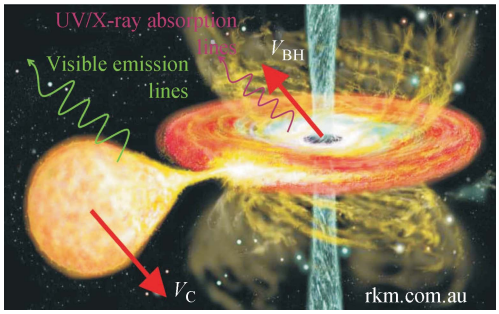

Fig. 1 Illustration of a BHXB and microquasar. X-ray emission is produced from the central hot accretion disk. A jet is normally observed in the radio band. The companion star may produce optical emission lines. The disk wind may be observed with UV/X-ray absorption lines.

scales [9]. Soon after, superluminal jets are observed from a BHXB GRS 1915+105 [10], which is also referred to as a microquasar. Nevertheless both BHXBs are quite unusual compared to many others, thus microquasars were considered quite unusual. However it became clear that microquasars may be quite common among BHXBs, since the discovery of a normal BHXB GRO J1655–40 [11], whose superluminal jets were observed [12] and showed some correlations with its X-ray emission [13]. Subsequently several more BHXBs have been observed with superluminal jets. At this stage *microquasars* began to be referred to as BHXBs with relativistic jets (with bulk motion of about or larger than 90% of the speed of light), to distinguish them from NS X-ray binaries (NSXBs) that only have mildly relativistic jets (with bulk motion of about or smaller than 50% of the speed of light) [14]. However the discovery of relativistic jets from a NSXB Circinus X–1 made the situation complicated: relativistic jets are no longer uniquely linked to BHs [15].

Now in retrospect, a *microquasar* can be literally and easily understood as the *micro* version of a quasar; however a quasar may or may not be observed with collimated jets. A quasar has been already understood as a special galaxy centered by an actively accreting supermassive BH with a mass from millions to billions of $M_\odot$, and thus its total light output is dominated by the BH's accretion process, in a similar way as in BHXBs. The production or lack of relativistic jets may have similar or even the same underlying physical mechanisms in BHXBs and AGNs, though their surrounding environments may modify their observed morphologies [16]. It is therefore more natural to simply refer *microquasars* as BHXBs; in the rest of this article, *microquasar* and *BHXB* are used interchangeably.

We therefore will focus on BHXBs and thus will not discuss binary systems producing gamma-rays and sometimes radio jets, which are most likely high-mass NSXBs and in which jets or pulsars' winds interact with the wind of its high-mass companion to produce the observed gamma-rays [17–23]. Such systems show very different observational characteristics, e.g. the long (1667 days) super-orbital modulation with phase offset (about 280 days) between its X-ray and radio light curves found in LS I+61°303 [24].

3 Review of reviews

Here I attempt to review the four recent review articles [1–4] I consider most useful to readers. Additional information and updates are provided when necessary. Some overlaps exists between these review articles, as expected and inevitable in bottom-up review articles. To avoid repetitions as much as possible in this article, I thus put different emphasizes on different articles, with of course my personal tastes and perceptions.

3.1 The most recent *Science* collection

The recent collection of perspectives and reviews in the *Science* magazine provides excellent introductions to and concise summaries of the current state of our understanding of BH physics and astrophysics [1, 25–27]. To the subjects of this article, the most relevant article in this collection is the one by Fender and Belloni entitled

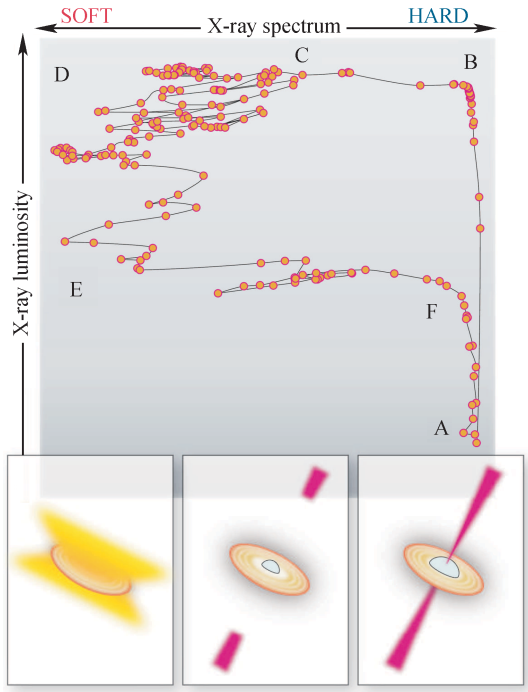

Fig. 2 A typical Hardness-Intensity-Diagram (HID) of spectral evolution of a BHXB, following the A→B→C→D→E→F cycle (top). Steady or transient jets are present during the A→B or B→C→D stage. No jets are observed, but hot disk winds are ubiquitous during the D→E stage. Reproduced from Ref. [1].

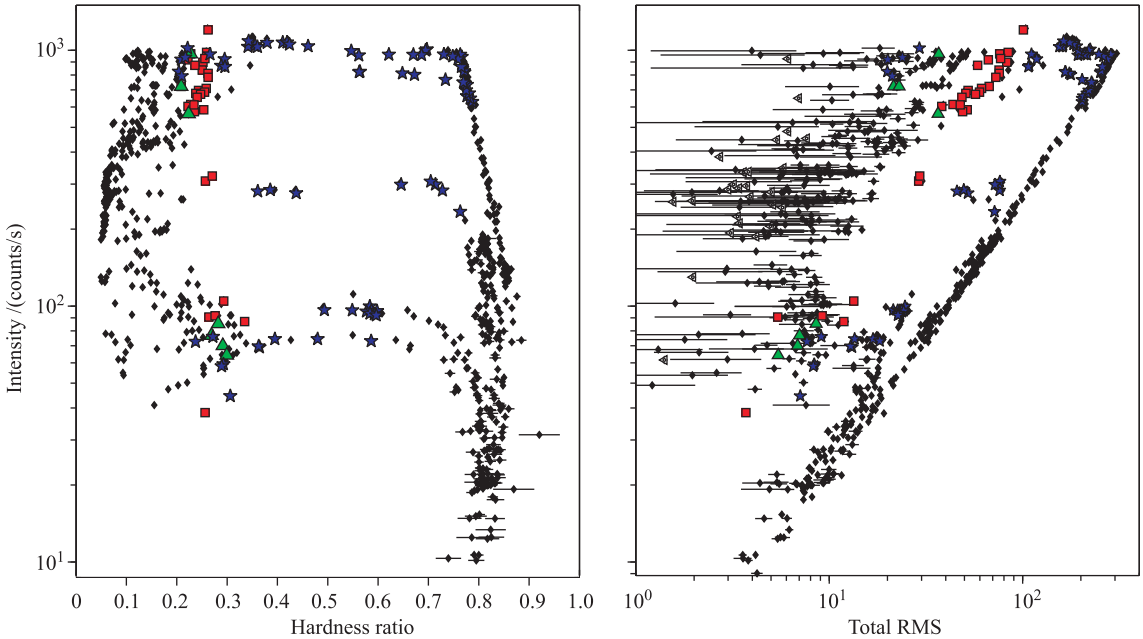

Fig. 3 The Hardness-Intensity-Diagram (HID) and RMS-Intensity-Diagram (RID) of the BHXB GX 339–4. The main difference from Fig. 2 is that there are additional horizontal tracks at intermediate intensities, a phenomenon known as hysteresis of state transitions, which will be discussed in Section 7. Reproduced from Ref. [28].

"Stellar-Mass Black Holes and Ultraluminous X-ray Sources", which is focused on the observational characteristics of BHXBs [1]. In particular, the article provides an excellent description of the general picture of spectral evolutions of BHXBs with the Hardness-Intensity-Diagram (HID), which is found to be well correlated with the observed jets from BHXBs, as shown in Fig. 2. Actually this cycle is also well tracked by their flux variability, represented by the measured root-mean-squares (rms) above its average flux, as shown by the RMS-Intensity-Diagram (RID) [28] of the BHXB GX 339–4 in Fig. 3, which also shows additional horizontal tracks at intermediate intensities. Sometimes, a full HID cycle does not go into the soft state at all (Fig. 4), perhaps due to a failed outburst [29].

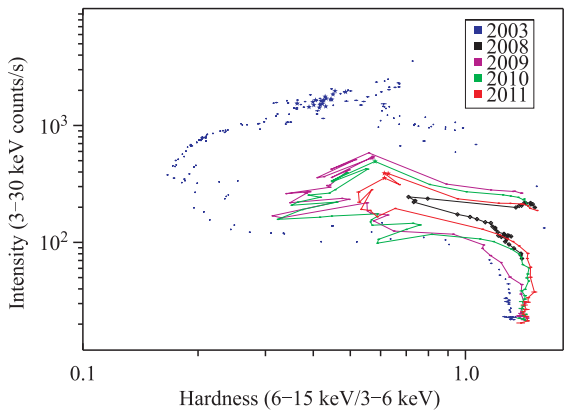

Fig. 4 The Hardness-Intensity-Diagram (HID) of H1743–322. The main difference from Fig. 3 is that there is a complete track at low intensity from the 2008 outburst, which did not go into the soft state at all. Reproduced from Ref. [29].

The basic scenario is as follows. During the initial stage of an X-ray outburst of a BHXB (A→B), which is triggered by a sudden increase of accretion rate onto the BH, its spectrum is normally hard and steady jets are always observed. After reaching its peak luminosity, its spectrum begins to soften in a chaotic way and transient jets are normally observed (B→C→D). After this transition, the system calms down with a soft spectrum and no jets are present (D→E). Finally the system returns to its quiescent state with a hard spectrum accompanied with the reappearance of jets (E→F). Throughout this cycle, the presence of hot accretion disk winds appears to be anti-correlated with its spectral hardness and jet ejection. This empirical pattern appears to be quite universal for all BHXBs with very few exceptions, though the underlying physics is still not well understood yet. Nevertheless putting together the above scenario is a very significant progress in this field over the last ten years. Due to the conciseness of this article, some other important subjects on BHXBs are not fully discussed and many original references are also missing.

Other articles in this collection [25–27] are less relevant to the subjects of this article, but are still quite interesting to read, within the context of BH astrophysics and physics. The only other type of astrophysical BHs known to exist in the physical universe are supermassive BHs in the center of almost each galaxy. Volonteri

[27] concisely summarized our current understanding on how they are formed and grow over the cosmic time; merging of two BHs is a key process here. Thorne [25] focused on what happens when BHs merge together to produce gravitational waves, which might be used as a new laboratory for studying gravitational physics and a new window for exploring the universe. Witten [26] then explained the quantum properties of BHs, in particular the basic ideas behind Hawking radiation, which might not be important at all for astrophysical BHs. Nevertheless the understanding gained through studying the quantum mechanics of BHs actually plays very important roles in developing other theories of physics, such as that in heavy ion collisions and high-temperature superconductors, as vividly described by Witten [26].

3.2 The most recent ARA&A article on BHXBs, with some updates

The most recent ARA&A article on BHXBs by Remillard and McClintock entitled "X-Ray Properties of Black-Hole Binaries" [2] (referred to as RM06 hereafter) provides the most complete, comprehensive and accurate review of BHXBs, which actually covers subjects much beyond just the X-ray properties of BHXBs. The *Introduction* of RM06 highlights the initial theoretical and observational studies of BHXBs, followed by brief comments on several main review articles on BHXBs preceding this one and the basic properties of BHs within the context of general relativity (GR). All main properties of BHXBs known at the time are summarized in the first table and figure there. In Table 2, I compile the most updated data on all BHXBs currently known, including three BHXBs outside the Galaxy and not in the Large Magellanic Cloud (LMC); the currently available spin measurements for these BHs are also included for completeness. In Table 2,

$$f(M) \equiv P_{\rm orb}K_{\rm C}^3/(2\pi G) = M_{\rm BH}\sin^3 i/(1+q)^2 \qquad (1)$$

where $P_{\rm orb}$ is the orbital period, $K_{\rm C}$ is the semi–amplitude of the velocity curve of the companion star, $M_{\rm BH}$ is BH mass, i is the the orbital inclination angle, and $q \equiv M_{\rm C}/M_{\rm BH}$ is the mass ratio. In Fig. 5, I show the updated graphical representation of most of the BHXBs listed in Table 2.

The X-ray properties of BHXBs are characterized by their X-ray light curves, timing and spectra. Essentially all known BHXBs were discovered initially as bright X-ray sources, and the majority of them were detected as transient X-ray sources with X-ray all-sky monitors. The transient properties of some of BHXBs can be interpreted by the disk instability model (DIM) (see Ref. [49] and

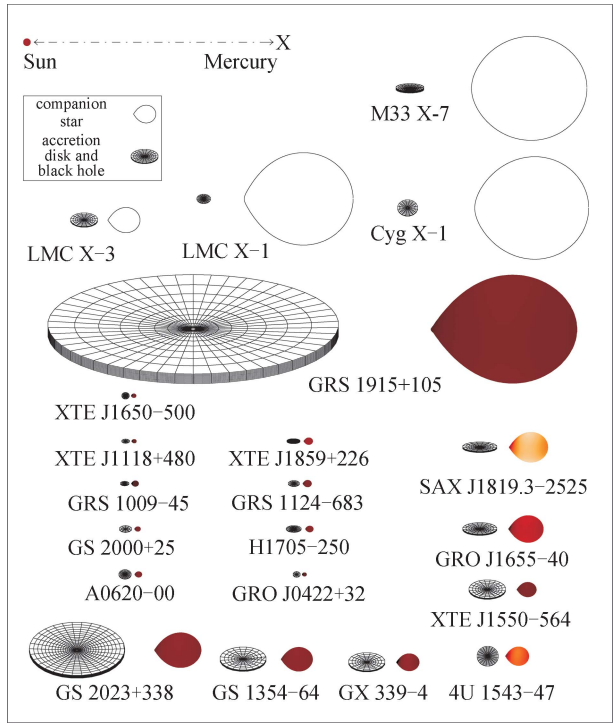

Fig. 5 Schematic diagram of the dynamically confirmed BHXBs, maintained by Dr. Orosz (http://mintaka.sdsu.edu/faculty/orosz/web/). The color scale for the 17 objects with low mass companions (i.e. stars with masses less than about $3M_\odot$) represents the temperature of the star. However, the high mass companions in Cyg X–1, LMC X–1, LMC X–3, and M33 X–7 are considerably hotter, and are thus not well represented in color scale. Adapted from the plot maintained by Dr. Orosz (http://mintaka.sdsu.edu/faculty/orosz/web/ and Fig. 1 in Ref. [48]).

references therein), which assumes a constant mass transfer rate from the mass donor to the accretion disk. However the accretion rate from the disk to the compact object, i.e., a white dwarf (WD), a neutron star (NS), or a BH, is normally lower than the mass supply rate in the disk, so mass is accumulated in the disk. When the accumulated mass exceeds a certain critical value, a sudden increase of accretion rate results in a nova-like outburst. DIM is most successful in explaining an outburst with fast rise and exponential decay (FRED). However as shown in RM06, many observed X-ray light curves of BHXBs are far more complicated than just FRED and their recurrent time scales are also not compatible with DIM. Perhaps disk truncation (a subject to be discussed extensively more later) and mass transfer instability are additional ingredients [50].

X-ray emission from a BHXB is variable at all time scales, from the free-fall or Keplerian orbital time scale of milliseconds near the BH, to the various oscillations (some are even related to GR) in the disk with time scales from milliseconds to minutes, to the viscous time scales of minutes, and to the various instabilities of different time

Table 2 Twenty four confirmed BHXBs and their BH masses and spins. Except those marked with references, all other data are taken from Remillard and McClintock [2] (references therein).

Coordinate name	Common[2)] name/prefix	$P_{\rm orb}$/hr	$f(M)/M_\odot$	$M_{\rm BH}/M_\odot$	a_*[1)] (cJ/GM^2)	a_*[2)] (cJ/GM^2)
0422+32	(GRO J)	5.1	1.19±0.02	3.7–5.0	−1[3)]	
0620–003	(A)	7.8	2.72±0.06	6.35–6.85 [30]	0[4)]	0.12±0.19 [31]
1009–45	(GRS)	6.8	3.17±0.12	3.6–4.7		
1118+480	(XTE J)	4.1	6.1±0.3	6.5–7.2		
1124–684	Nova Mus 91	10.4	3.01±0.15	6.5–8.2	−0.04	
1354–64	(GS)	61.1	5.75±0.30	–		
1543–475	(4U)	26.8	0.25±0.01	8.4–10.4		0.75–0.85 [32]
1550–564	(XTE J)	37.0	6.86±0.71	8.4–10.8		0.06–0.54 [33]
1650–500	(XTE J)	7.7	2.73±0.56	–		
1655–40	(GRO J)	62.9	2.73±0.09	6.0–6.6	0.93[5)]	0.65–0.75 [32]
1659–487	GX 339–4	42.1	5.8±0.5	–		
1705–250	Nova Oph 77	12.5	4.86±0.13	5.6–8.3		
1743–322	(H)	–	–	–		0.2±0.3 [34]
1819.3–2525	V4641 Sgr	67.6	3.13±0.13	6.8–7.4		
1859+226	(XTE J)	9.2	7.4±1.1[5)]	7.6–12.0		
1915+105	(GRS)	804.0	9.5±3.0	10.0–18.0	0.998	0.98–1.0 [35]
1956+350	Cyg X–1	134.4	0.244±0.005	13.8–15.8 [36]	±0.75[6)]	> 0.95 [37]
2000+251	(GS)	8.3	5.01±0.12	7.1–7.8	0.03	
2023+338	V404 Cyg	155.3	6.08±0.06	10.1–13.4	−1[3)]	
0538–641	LMC X–3	40.9	2.3±0.3	5.9–9.2	−0.03	< 0.3 [38]
0540–697	LMC X–1	93.8	0.13±0.05	9.4–12.5 [39]		0.94–0.99 [40, 41]
0020+593	IC 10 X–1	34.9	7.64±1.26	> 20 [42, 43]		
0055–377	NGC 300 X–1	32.3	2.6±0.3	> 10 [44]		
0133+305	M33 X–7	82.9	0.46±0.07	14.2–17.1 [45]		0.84±0.05 [46]

[1)] Reported in the first paper on systematic BH spin measurements [47];
[2)] Reported in the most recent literature;
[3)] Postulated to be extreme retrograde Kerr BH, due to the lack of the thermal disk component above 2 keV (GRO J1719–24 also belongs to this class) [47];
[4)] Postulated to be non-spinning BH, due to the observed low disk temperature;
[5)] BH mass of 7 $M_\odot$ assumed [47];
[6)] Based on the inner disk radius decrease by a factor of two from the hard state to the soft state transition [47].

scales. Therefore timing studies of BHXBs can probe the geometry and dynamics in BHXBs. However, lack of coherent signals, such as that observed from pulsars, makes it difficult to unambiguously identify the underlying mechanisms from the detected X-ray variabilities. Nevertheless power density spectra (PDS) and rms still allow us to make progress in understanding the general characteristics of a BHXB, in particular when combined with its spectral behaviors, as already discussed briefly above.

The most successful understanding of BHXBs so far is the description of their thermal X-ray spectral component by the classical Shakura–Sunyaev Disk (SSD) model [51]. After applying GR to SSD, the temperature distribution in the disk can be obtained [52]. Applying this model to BHXBs, one can even measure the spin of their BHs [47], by assuming that the inner accretion disk boundary is the inner-most stable circular orbit (ISCO) of the BH (a subject to be discussed more in Section 4). However a power-law (PL) component is almost ubiquitous in the spectra of BHXBs. The interplay between these two components results in various spectral states, which are also found to be well correlated with their timing properties.

Historically these spectral states have been named in many different ways, reflecting mostly how they were identified with the observations available at the times. In RM06, three states are defined, which show distinctively different spectral and timing behaviors, as shown in Fig. 6 based on the RXTE data on the BHXB GRO J1655–40. The *thermal state* has its X-ray spectrum dominated by the thermal disk component and very little variability. The *hard state* has its X-ray spectrum dominated by the a PL component and strong variability. The *steep power-*

law (SPL) state is almost a combination of the above two states, but the PL is steeper. I will keep using these definitions throughout this article for consistency. Please refer to Table 2 in RM06 for quantitative descriptions of these three states. When a BHXB is in quiescence, i.e., not in an outburst, its spectral shape is similar to the hard state spectrum.

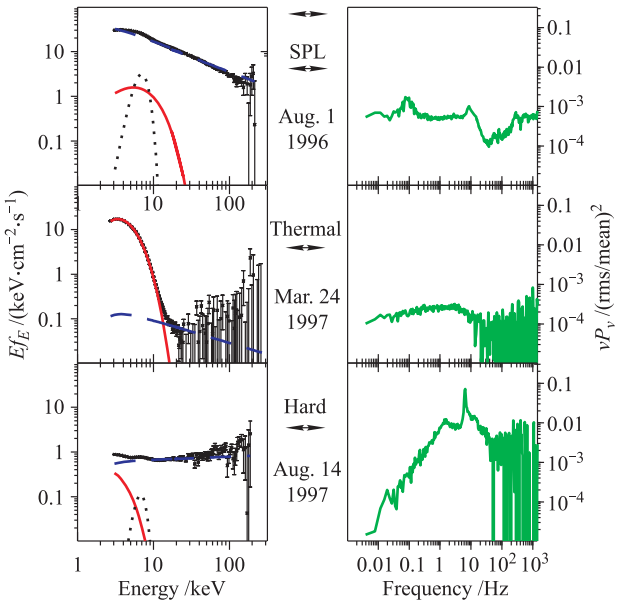

Fig. 6 Characteristic spectra and PDS of the BHXB GRO J1655–40 in three different states, namely, steep power-law (SPL), thermal and hard states. Please refer to Fig. 2 in RM06 for details. Reproduced from Ref. [2].

Referring back to Fig. 2, RM06 found that the HID can be reasonably well understood in terms of transitions between the above three states; I summarize this in Table 3. After examining the extensive RXTE data on spectral evolutions of six BHXBs, the above conclusion seems to be valid generally. Thus a coherent picture seems to emerge: jets are produced only when the PL component in the spectrum is strong and winds are present only when the PL component disappears; jets and winds appear to be mutually exclusive. This suggests that transient winds should appear in the SPL state, anti-phased with transient jets, if winds quench jets as suggested recently [53, 54].

Table 3 Relations between HID, spectral states, jets and wind.

HID stage	State transition	Jets	Winds
A→B	hard→SPL	steady	no
B→C→D	SPL→soft	transient	transient?
D→E	soft decay	no	steady
E→F	soft→hard	steady	no

The robust link between the PL component and jets provides an important clue to the jet production mechanism. The PL component is believed to be produced in an optically thin and geometrically thick corona, in which hot electrons up-scatter the thermal photons from the disk. As discussed in RM06, the inner region of the disk appears to be truncated quite far away from the BH in the hard state; this should be the primary reason for the low luminosity of this state, as evidence for the existence of BHs in BHXBs. However it is still not understood how the corona is formed; I will discuss this later in Section 6.

In the final part, RM06 discussed the exciting possibilities of using BHXBs as probes of strong gravity, including confirming these BHXBs contain true BHs, measuring the spins of BHs, relating BH spin to the Penrose process and other phenomena, and finally carrying out tests of the Kerr Metric. They also discussed in length how to measure the spins of BHs and commented the various methods of doing so. In Section 7 I will re-visit the BH spin measurements in details.

Lacking of a solid surface, a BHXB is not expected to produce and actually never observed to have coherent pulses. However quasi-periodic oscillations (QPOs) are frequently detected in their X-ray light curves; a QPO is defined as a "bump" feature in the PDS, if $Q = \nu/\Delta\nu > 2$, where ν and $\Delta\nu$ are the peak frequency and FWHM of the bump, respectively. The observed QPOs are further divided into low frequency (LF) (0.1–30 Hz) and high frequency (HF) (> 30 Hz) QPOs. Typical LFQPOs can be found as the peak around several Hz in the top and bottom PDS of Fig. 6. In literature, LFQPOs are further divided into several subclasses and their underlying mechanisms are far from clear at this stage, though many models have been proposed and briefly discussed in RM06. HFQPOs have been detected from several sources at 40–450 Hz. Of particular interests are their stable nature when detected, which may be linked to either the mass or spin or both of the BH in a BHXB.

In some cases a 3:2 frequency ratio is found. Although the 3:2 HFQPO pairs could be interpreted in some epicyclic resonance models [55, 56], there remain serious uncertainties as to whether epicyclic resonance could overcome the severe damping forces and emit X-rays with sufficient amplitude and coherence to produce the HFQPOs. A revised model applies epicyclic resonances to the magnetic coupling (MC) of a BH's accretion disk to interpret the HFQPOs [57]. This model naturally explains the association of the 3:2 HFQPO pairs with the steep power-law states and finds that the severe damping can be overcome by transferring energy and angular momentum from a spinning BH to the inner disk in the MC process.

3.3 Two comprehensive and long articles on modeling accretion flows in BHXBs

Page limitations to the above review articles did not allow in depth discussions on the detailed processes and models of accretion flows in BHXBs, which are responsible for the above described energy spectra, PDS, state transitions, jets, and wind. Here I introduce two comprehensive and long articles just on this, by Done [3] and Done, Gierliński & Kubota [4].

3.3.1 A beginner's guide

The first is intended to readers who just start research in this field [3]. It started with the basic tools in plotting spectra and variability, and then described the basic ideas and methods used to infer the inner accretion disk radius when a BHXB is in a thermal state, in order to measure the BH spin [47]. A useful introduction is made on how to make various corrections to account for various effects, including color correction, special and general relativistic effects, starting from the original work [47]. Several commonly use fitting models, i.e., DISKBB, BHSPEC and KERRBB, in the XSPEC package are also briefly introduced. An example is given to demonstrate that the expected relation $L_{\rm disk} \propto T_{\rm in}^4$ [47] agrees with the data from the BHXB GX 339–4 [58], where $L_{\rm disk}$ and $T_{\rm in}$ are the disk's total luminosity and temperature at the inner disk boundary, respectively.

The hard state is then briefly touched upon, using the Advection Dominated Accretion Flow (ADAF) model [59]. ADAF naturally explains the hot corona required by the observed PL component, especially at very low accretion rate. Evaporation at low accretion rate in the inner disk region has been proposed as the mechanism producing a geometry with a radially truncated disk and a hot inner flow; the latter might be the ADAF [60]. This also means that when a significant PL component is present in the spectrum, BH spin measurement cannot be done with the inferred inner disk boundary (see, however, counter evidence discussed in Sections 4 and 6). This geometry is considered a paradigm that can account for many of the observed diverse phenomena from spectral evolution to timing properties.

A brief, yet interesting discussion is given on scaling up the above models to Active Galactic Nuclei (AGNs), which host actively accreting supermassive BHs in the centers of galaxies. Applying the insights learnt from BHXBs on their spectral evolution, changing disk-temperature with accretion rate and BH mass, and disk-jet connections, one might be able to understand many phenomena beyond the simple AGN unification scheme, in which the different observational appearance is all attributed to an viewing angle difference.

The continuum emissions of both the disk thermal and PL components are modified by absorptions and added by additional spectral features along the line of sight (LOS). Absorptions in neutral media produce various photoelectric absorption edges, but in ionized media result in both absorption edges and lines. In addition to recovering the original X-ray emission of a BHXB, modeling the absorption features is important in learning the physical properties of the absorption media, such as column density, ionization and velocity along LOS. Winds from BHXBs discussed above are always detected this way. Several XSPEC fitting models for various kinds of absorption edges and lines are also introduced here, i.e. TBABS, ZTHABS, TBVARABS, ZVPHABS,

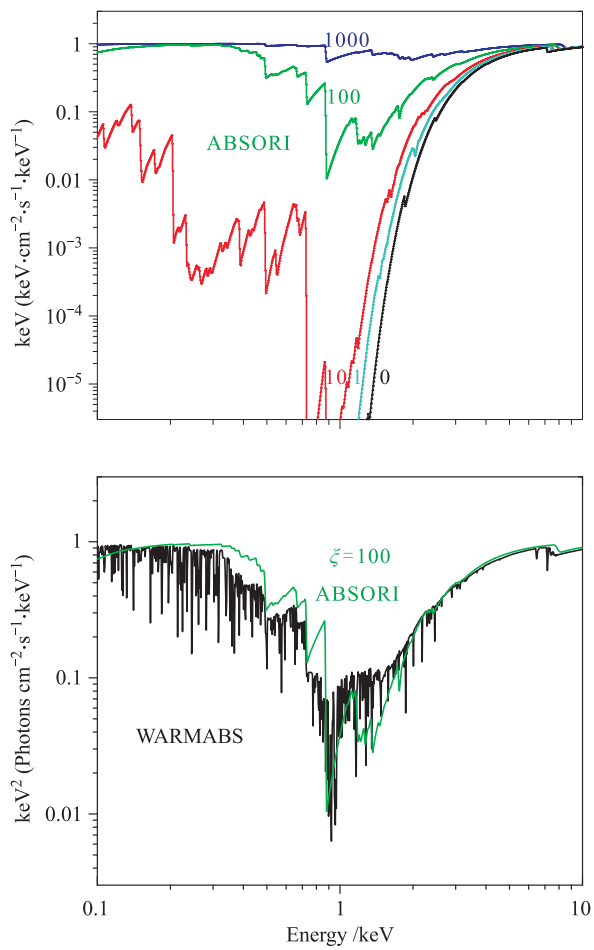

Fig. 7 Calculated absorption structures of a column density $N_{\rm H} = 10^{23}$ cm^{-2} for different ionization parameter $\xi = L/nr^2$, where L is the illuminating luminosity, n is the density of the medium, and r is the distance from the radiation source. *Top panel*: with the ABSORI model that does not include absorption lines. *Bottom panel*: for $\xi = 100$ with both ABSORI and WARMABS, the latter is based on the XSTAR photo-ionization package thus absorption lines are taken into account properly. Reproduced from Ref. [3].

TBNEW, ABSORI and WARMABS. Figure 7 shows the calculated absorption structures with ABSORI and WARMABS; note that ABSORI does not include absorption lines, but WARMABS does.

X-rays interacting with the surrounding medium can ionize it and heat the free electrons up by Compton scattering; hot electrons can also loose energy by interacting with lower energy photons. A Compton temperature of the plasma is reached when the above two processes reaches an equilibrium. The temperature is determined by only the spectral shape of the continuum, so the heated plasma can escape as winds from the disk if the velocity of the ions exceed that of the escape velocity at that radius, which is usually very far away from the inner disk boundary. As the continuum luminosity approaches the Eddington limit, the radiation pressure reduces the escape velocity substantially in the inner disk region such that continuum driven winds can be launched almost everywhere in the disk of a BHXB, forming a radiation driven wind, which is also called thermal wind; alternatively winds may also be driven magnetically in the inner disk region, but this is much less understood yet. In contrast, in an AGN the peak continuum emission is in the UV band, which has a much larger opacity than Compton scattering in neutral or weakly ionized medium during both photoelectric and line absorptions. This means the effective Eddington luminosity is reduced by large factors and UV line driven wind is easily produced at high velocity. This explains the relatively lower velocity (hundreds km/s) and highly ionized winds from BHXBs, but much higher velocity (thousands km/s to $0.2c$) and weakly ionized winds from AGNs.

Material illuminated by X-rays produce both fluorescence lines and reflection features, which depends on both the continuum spectral shape and ionization state of the material, as shown in Fig. 8 calculated with the XSPEC ATABLE model REFLIONX.MOD, which includes the self-consistent line and recombination continuum emission. Note that for highly ionized reflection, the Compton heated upper layers of the disk broadens the spectral features; these effects are not included in the simpler XSPEC model PEXRIV. Replacing the stationary slab by a disk around a BH, both the special and general relativistic effects will further smear (broaden) the spectral features, as shown in Fig. 9 for the iron line region with different values of ξ, inner disk radius $r_{\rm in}$, and viewing angle i; these are calculated with the REFLIONX.MOD and then convolved with KDBLUR in the XSPEC package. Other similar XSPEC fitting models are DISKLINE, LAOR, and KY. The inner disk radius can in principle be determined by modeling the observed broad iron line features, that in turn can be

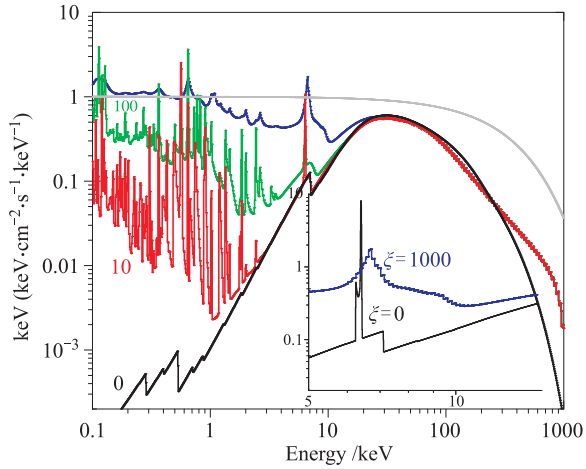

Fig. 8 Ionized reflections from a constant density slab, calculated with the XSPEC ATABLE model, REFLIONX.MOD, which includes the self-consistent line and recombination continuum emission, for different values of ξ. The inset shows a detailed view of the iron line region. For neutral material, around 1/3 of the line photons are scattered in the cool upper layers of the disk before escaping, forming a Compton down-scattered shoulder to the line. For highly ionized reflection, the upper layers of the disk are heated to the Compton temperature so that the spectral features are broadened. Reproduced from Ref. [3].

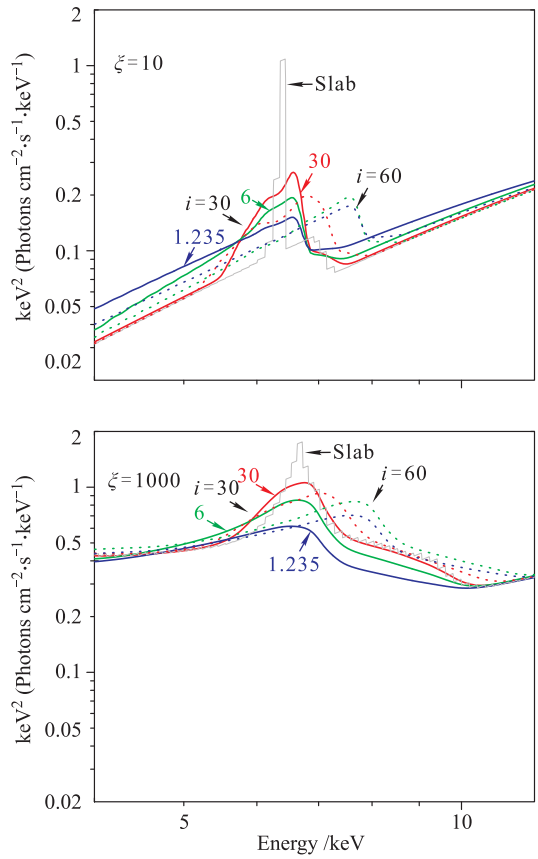

Fig. 9 Relativistic smearing of the iron line region. The sharp peak shown in solid grey lines are the original features. Other colored solid lines have different $r_{\rm in}$ marked in units of $r_{\rm g} = GM/c^2$ for $i = 30°$ (*solid lines*); similarly those for $i = 60°$ are shown in dotted lines. Reproduced from Ref. [3].

used to measure BH spins, as will be discussed briefly in Section 4. Figure 10 shows all components of a broad band spectrum of a BHXBs, including interstellar absorption.

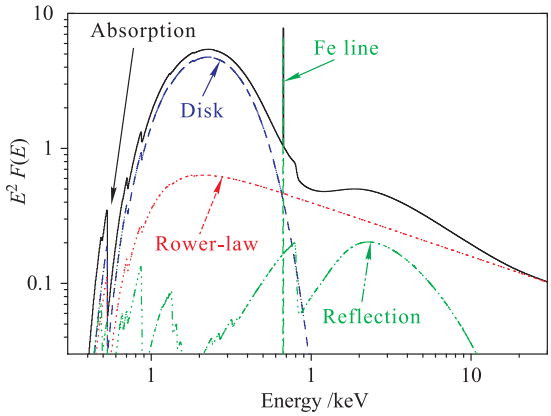

Fig. 10 Illustration of all components of the broad band energy spectrum of a BHXBs; interstellar absorption is normally prominent at low energies. Reproduced from Ref. [61].

We thus have two ways discussed so far to determine $r_{\rm in}$ of BHXBs by either fitting its thermal continuum or the fluorescent iron line feature. However results are not always consistent, obtained with different methods, even using the same data by different authors. The author believes that $r_{\rm in}$ increases at low accrete rate, to make room for the corona occupying this space. Nevertheless a fairly good summary on the current conflicts and confrontations is made on this issue, which I will discuss further in Section 4.

3.3.2 An expert's handbook

The second one can be considered as a handbook on accretion flows on BHXBs, and really lives up to its subtitle "Everything you always wanted to know about accretion but were afraid to ask" [4] (DGK07 hereafter). Besides its much longer length of 66 pages, the main difference from the above review articles is that it is focused on confrontations between theories and observations and intends to depict a coherence picture of the accretion physics in BHXBs. In the following I will summarize briefly the main points and conclusions reached in DGK07; those I have reviewed above and will discuss more later will be skipped for brevity.

The underlying physics of DIM for triggering the outbursts in BHXBs discussed above is the hydrogen-ionization instability, which produces the so-called "S"'-curve, as shown in Fig. 11; irradiation by the inner hot disk to keep the outer disk hot is required to produce the slow flux decays, e.g. the exponential decays, frequently observed in them. The outer disk radius is obviously another key parameter, which is determined by the tidal instability in a binary system. This mechanism can explain why BHXBs with high mass companions are all persistently bright, since their outer disks are always in the upper branch due to the combination of their higher average mass transfer rate and inner disk irradiation. Similarly it also explains the differences and similarities between the light curve properties of neutron star X-ray binaries (NSXBs) and BHXBs, since an NS has a lower mass. It should be noted that the additional surface emission from the NS may also help to maintain the outer disk hot and stay in the upper stable branch [62].

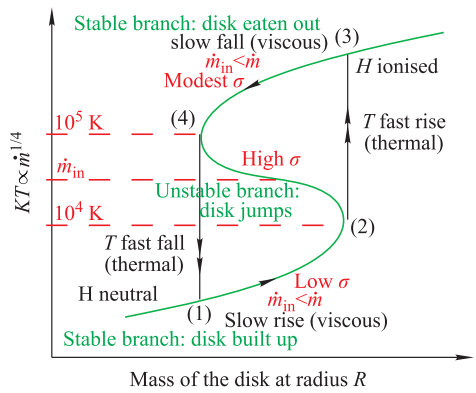

Fig. 11 "S"-curve due to the Hydrogen-ionization instability. At a radius R, the SSD solution gives $kT \propto \dot{m}^{1/4}$, where T is the local disk temperature and $\dot{m}$ is the local mass accretion rate. A positive slope means cooling can balance heating, so T changes slowly and the disk is stable. In the unstable middle branch, thermally emitted photons are absorbed to ionize the hydrogen atoms and are thus trapped in the disk, causing a large opacity (σ). If the mass supply rate $\dot{m}_{\rm in}$ happens in the middle range, then the disk experiences a limit-cycle instability from (1) to (4): (1) $T < 10^4$ K, neutral hydrogen has low σ, $\dot{m}_{\rm in} > \dot{m}$, so the disk is built up and T increases slowly; (2) $T \sim 10^4$ K, hydrogen atoms begin to be ionized and so has high σ, T increases rapidly until hydrogen is fully ionized; (3) $T > 10^5$ K, ionized hydrogen has modest σ, $\dot{m}_{\rm in} < \dot{m}$, so the disk is eaten out and T decreases slowly; (4) $T \sim 10^5$ K, protons and electrons begin to recombine, T decreases rapidly until reaching the lower stable branch again. Reproduced from Ref. [4].

The SSD prescription assumes that the stress is proportional to pressure. Because the gas pressure is $P_{\rm gas} \propto T$ but radiation pressure is $P_{\rm rad} \propto T^4$, so a small temperature increase causes a large pressure increase when $P_{\rm rad} \geqslant P_{\rm gas}$, and thus large stress increase, which in turn heats the disk even more. The opacity cannot decrease effectively to cool it down, so the disk becomes unstable when $L \geqslant 0.06 L_{\rm Edd}$, where $L_{\rm Edd}$ is the Eddington luminosity of a BHXB. However in most BHXBs their disk emissions appear to be stable up to around $0.5 L_{\rm Edd}$. One way out is to assume that the stress is proportional to $\sqrt{P_{\rm rad} P_{\rm gas}} \propto T^{5/2}$, so the stress increases slower in

the radiation pressure dominated regime. Beyond this the disk should become unstable, as evidenced by the sometimes "heart-beat" bursts of the super-Eddington BHXB GRS 1915+105; other BHXBs with $L_{\rm max} > L_{\rm Edd}$ (e.g. V404 Cyg and V4641) were not observed with such instabilities, perhaps due to the combination of insufficient observational coverage and sensitivity. However similar "heart-beat" bursts were also observed recently from IGR J17091–3624, which is likely substantially sub-Eddington unless it is located much beyond 20 kpc and/or its BH mass is quite small [63].

Super-Eddington accretion flow (SEAF) can become stable again, if the radiation instability is overcome by an optically thick ADAF, i.e., the slim disk model, in which the trapped photons in the flow is advected inwards, thus balancing the heating generated by viscosity. Strong radiation driven winds can be easily produced; this can happen in BHXBs and NSXBs (e.g. Z-sources). Evidence exists that truncated inner disk (TID) is quite common in SEAF and outflow even dominates over inflow in SEAF [64].

The observed PL component in BHXBs cannot be explained by the SSD-like models and thus requires a hot accretion flow (HAF). At low accretion luminosity (e.g. the quiescent state), the HAF may be the advection dominated accretion flow (ADAF), the convection dominated accretion flow (CDAF), or the advection dominated accretion inflow/outflow solution (ADIOS). At higher luminosity (e.g. the hard state), the original hot and optically thin disk solution (i.e., the SLE solution) is unstable, because the electron heating efficiency by the Coulomb coupling between protons and electrons is too low. The luminous HAF (LHAF), however, has the advection as a heating source to electrons, so the heating efficiency increases and thus electrons can cool the flow more effectively. Outflows can be produced in ADAF/ADIOS; collimated jets can also be produced if magnetic fields are involved, so an accretion flow may even be jet dominated (i.e., JDAF).

The interplays between the SSD and HAF may be responsible for the observed different states in BHXBs discussed above. If the PL component is produced by Compton up-scattering, then the combination of the optical depth τ and $\mathcal{L}_{\rm h}/\mathcal{L}_{\rm s}$, where $\mathcal{L}_{\rm h}$ is the heating power in electrons and $\mathcal{L}_{\rm s}$ is the cooling power in seed photons, can describe the observed variety of spectra. For example, the hard state has $\mathcal{L}_{\rm h}/\mathcal{L}_{\rm s} \gg 1$, but the thermal and SPL state have $\mathcal{L}_{\rm h}/\mathcal{L}_{\rm s} \leqslant 1$. The location of $r_{\rm in}$ is proposed to be closely related to $\mathcal{L}_{\rm h}/\mathcal{L}_{\rm s}$, as illustrated in Fig. 12. As discussed above, the steeper PL in the thermal and SPL states is mostly non-thermal in nature, so non-thermal Comptonization is required. Detailed comparisons with data suggest thermal Comptonization also cannot be ignored even in the thermal and SPL states.

In Fig. 12, the hot inner flow (HIF) and patchy corona are responsible for thermal and non-thermal Comptonization, respectively. When a source transits from hard to SPL state, $r_{\rm in}$ decreases, HIF is reduced but the patchy corona becomes dominant. The transition from SPL to soft state is then marked by the disappearance of HIF and significant reduction of the patchy corona. The above scenario obviously depends on two fundamental assumptions: i) slab-HIF produces the non-thermal PL component; ii) slab-HIF is mostly located between the

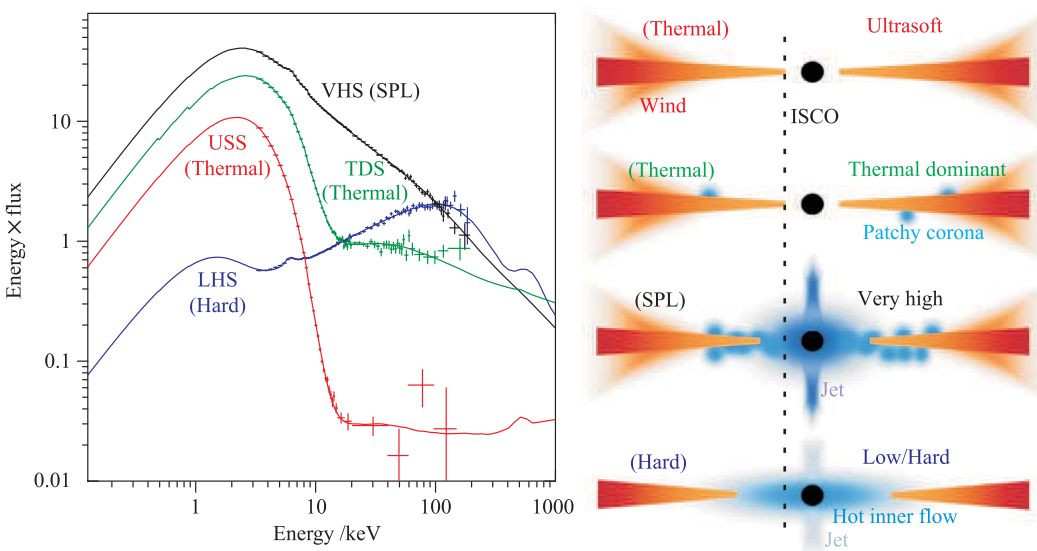

Fig. 12 *Left panel*: A selection of spectra in different states taken from the 2005 outburst of GRO J1655–40; state names in parentheses are defined in RM06. *Right panel*: Proposed accretion flow structures in these different spectra; note the SSD is truncated away from ISCO in the bottom two states. Reproduced from Ref. [4].

TID and the BH. Both assumptions are examined exhaustively based on the existing observations and their spectral modeling. Slab-HIF is found to be consistent with essentially all data. An alternative to slab-HIF is that the PL is produced from the jet base and beamed away from the disk; however observations suggest the PL emission is quite isotropic, thus in conflict with this. TID is found also consistent with data when the PL component becomes important, since the observed $L_{\rm disk} \sim T_{\rm in}^4$ deviates significantly from a linear relation, suggesting $r_{\rm in}$ is larger when the PL component becomes important. However some studies showed that $r_{\rm in}$ is unchanged in the initial hard state, if the Compton up-scattering process is treated properly in Monte-Carlo simulations to recover the lost disk photons [65]; this issue will be further discussed in Section 4.

The above developed HIF/TID model based on the spectral evolutions of BHXBs can also be applied to explain the majority of time variability PDS of BHXBs consistently. The TID acts as a low pass filter as it cannot response effectively to variations in the HIF, so $r_{\rm in}$ controls the low frequency break of the PDS: $\nu_{\rm LFB} \sim 0.2(r/6)^{-3/2}(m/10)^{-1}$ Hz, where $r = r_{\rm in}/r_{\rm g}$ and $m = M_{\rm BH}/M_\odot$; this predicts that $\nu_{\rm LFB}$ changes from 0.03 to 0.2 Hz as observed during transitions from the hard to SPL and soft states if r decreases from 20 to 6. The HIF/TID model can also explain the observed LFQPO variations with luminosity, if the LFQPOs are some kinds of characteristic frequencies related to $r_{\rm in}$. To some extend, the shape of the PDS can also be explained by this model. However the observed variability rms $\sim$ flux linear correlation and log-normal distribution of fluctuations may need additional ingredient, such as the proposed propagation fluctuation model. However I point out that such correlations and distributions are also observed in the light curves of gamma-ray bursts and solar flares [66, 67], which can be produced by the generic self-organized criticality mechanism [66]. Similar rms $\sim$ flux correlation has also been found for blazars, in agreement with the minijets-in-a-jet statistical model [68].

The spectral and timing properties of weakly magnetized NSXBs are known to have many similarities and differences from BHXBs; this is particularly true for the atoll sources that have similar ranges of $L/L_{\rm Edd}$ to BHXBs. The essential distinction is that an NS has a solid surface, but a BH does not. Observationally the continuum spectra of atoll sources can be modeled as composed of SSD, PL emission, and blackbody emission from the NS surface (or the boundary layer between the TID and NS surface); the former two components are quite similar to BHXBs. The spectral evolutions of these NSXBs are thus driven similarly by the combinations of τ and $\mathcal{L}_{\rm h}/\mathcal{L}_{\rm s}$. However the blackbody emission is an additional source of $\mathcal{L}_{\rm s}$, so the PL is not as hard as that in BHXBs and $r_{\rm in}$ variations are less effective in changing $\mathcal{L}_{\rm h}/\mathcal{L}_{\rm s}$; the latter means it is more difficult to find evidence of TID from modeling only the spectral evolutions in NSXBs. On the other hand, the TID/HIF model in NSXBs can produce timing behaviors in the same way as in BHXBs discussed above, consistent with observations; additional timing behaviors, such as coherent X-ray pulsations and kilo-Hz QPOs observed in these NSXBs, are caused by the rapid spins of the hard surfaces of the NSs.

4 Further developments on BH spin measurements

A BH predicted in GR can only possess three parameters, namely, mass, spin and electric charge, known as the so-called BH no hair theorem. Even if a BH was born with net electric charge, its electric charge can be rapidly neutralized by attracting the opposite charge around it in any astrophysical setting, because the strength of electromagnetic interaction is many orders of magnitude stronger than that of gravitational interaction. Therefore an astrophysical BH may only have two measurable properties, namely, mass and spin, making BHs the simplest macroscopic objects in the universe. Practically, only Newtonian gravity is needed in measuring the BH mass in a binary system. However, GR is needed in measuring the BH spin.

The mass and spin of a BH has different astrophysical meanings. Its mass can be used to address the question of "*How much* matter (and energy) has plunged into the BH?". However its spin can be used to address the question of "*How did* the matter (and energy) plunge into the BH?". This is because matter and energy plunged into a BH can carry angular momentum, which is a vector with respect to the spin axis of the BH. In order to increase the total gravitating mass-energy from $M_{\rm i}$ with zero spin to $M_{\rm f}$, the added rest-mass must be [69, 70]

$$\Delta M = 3M_{\rm i}\left(\arcsin\frac{M_{\rm f}}{3M_{\rm i}} - \arcsin\frac{1}{3}\right) \tag{2}$$

and its final spin becomes

$$a_* \equiv \frac{cJ}{GM_{\rm f}^2} = \left(\frac{2}{3}\right)^{1/2}\frac{M_{\rm i}}{M_{\rm f}}\left[4 - \left(\frac{18M_{\rm i}^2}{M_{\rm f}^2} - 2\right)^{1/2}\right] \tag{3}$$

where J is the BH's angular momentum. Clearly we have $a_* = 1$ when $M_{\rm f}/M_{\rm i} = 6^{1/2}$; further accretion simply maintains this state [70]. Therefore the required additional rest-mass to spin a BH from zero to maximum spin is $\Delta M \simeq 1.85M_{\rm i} = 0.75M_{\rm f}$; this is a lower limit to

the accreted mass [71]. Figure 13 shows a_* as a function of ΔM. Ignoring Hawking radiation of a macroscopic BH, the only way to extract the energy of a BH and thus reducing its gravitating mass is by extracting its spin energy. Recently, evidence of BH spin energy extraction to power relativistic jets has been found, from the observed correlation between the maximum radio luminosity and its BH spin of a microquasar [72, 73]; however the average jet power is not correlated with BH spin [74]. This indicates that jets may be produced by both Blandford–Payne (BP) [75] and Blandford–Znajek (BZ) [76] mechanisms; but the BZ mechanism is more powerful and responsible for producing the peak radio luminosity. This provides another possible way to estimate a BH's spin [73], similar to a recent proposal of using the peak luminosity of the disk emission to estimate a BH's spin [77]. However there is so far no independent demonstration of validness of either of the above two new methods, which are thus not discussed further in this section.

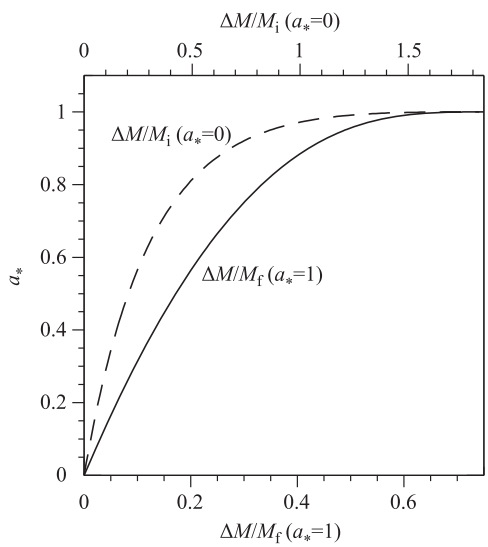

Fig. 13 BH spin a_* vs. accreted rest-mass ΔM, in units the final mass $M_{\rm f}(a_*=1)$ (*solid line*, bottom axis), and in units of the initial mass $M_{\rm i}(a_*=0)$ (*dashed*, top axis). Reproduced from Ref. [71].

Figure 14 shows the mass reduction, $\Delta m = (M_{\rm max} - M_{\rm f})/M_{\rm max}$ ($M_{\rm max}$ and $M_{\rm f}$ are the BH's maximum mass and final mass, respectively), as a function of extracting efficiency ϵ of an extreme Kerr BH. For a $10M_\odot$ BH with $\epsilon = 1$ ($\Delta m \sim 0.3$), the total extracted energy is $\Delta m M_{\rm f} c^2 \simeq 10^{54}$ erg and its total gravitating mass is reduced to $M_{\rm max}/\sqrt{2}$ [71]; this energy could be sufficient to power gamma-ray bursts (GRBs). It is thus plausible that supercritical accretion onto a newly born BH may spin it up and extract its spin energy to power ultra-relativistic jets; multiple spin-up and spin-down cycles may also happen during one GRB, if the collapsing material is clumpy.

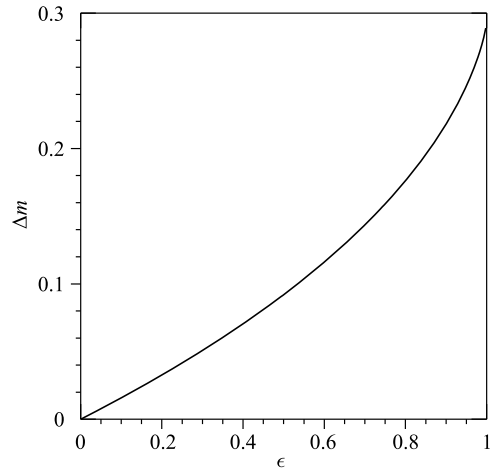

Fig. 14 Extracted fractional energy $\Delta m = (M_{\rm max} - M_{\rm f})/M_{\rm max}$ as a function of efficiency ϵ of extraction of a BH's rotational energy. Reproduced from Ref. [71].

As shown in Fig. 15, the radius of the ISCO of the BH, $R_{\rm ISCO}$, is a monotonic function of the BH spin [78], beyond which radius a test particle will plunge into the BH under any perturbation; however, in Newtonian gravity a stable circular orbit can be found at any radius. It is thus reasonable to assume that the accretion disk around a BH terminates at this radius, i.e., $r_{\rm in} = R_{\rm ISCO}$. Therefore, a_* can be inferred if one can measure $R_{\rm ISCO}$ in units of its gravitational radius $r_{\rm g} = GM/c^2$. Currently three methods have been proposed to measure the BH spin in BHXBs, and all these methods rely essentially on measuring $R_{\rm ISCO}$. In case the radiative efficiency ($\eta \equiv L/\dot{M}c^2$) can be measured, a_* can also be

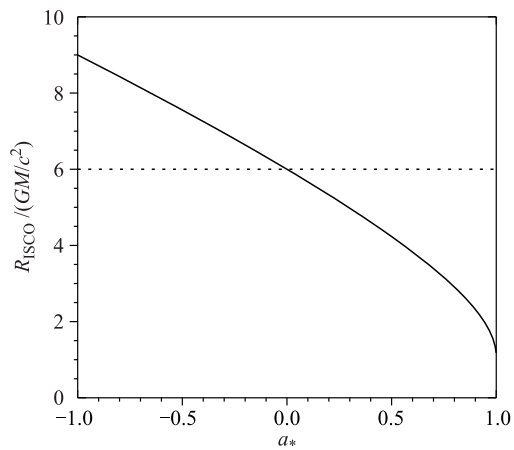

Fig. 15 The radius of the innermost stable circular orbit ($R_{\rm ISCO}$) of a BH as a function of the spin parameter (a_*) of the BH, i.e., the dimensionless angular momentum; a negative value of a_* represents the case that the angular momentum of the disk is opposite to that of the BH, i.e., the disk is in a retrograde mode. Therefore a_* can be measured by determining the inner accretion disk radius, if the inner boundary of the disk is the ISCO of the BH.

determined this way, as shown in Fig. 16. Actually η is a very simple function of $R_{\rm ISCO}$, i.e, $\eta \sim 1/R_{\rm ISCO}$, as shown in Fig. 17.

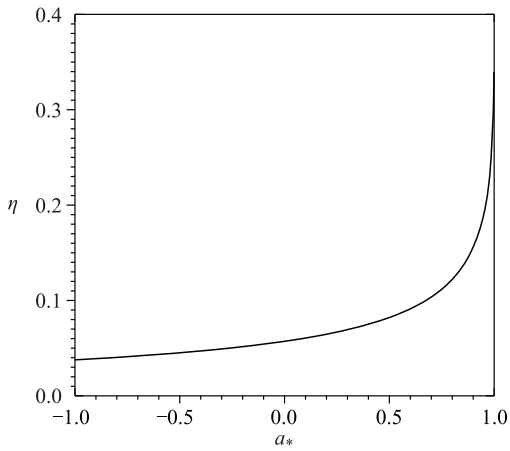

Fig. 16 Radiative efficiency η as a function of BH spin parameter a_*.

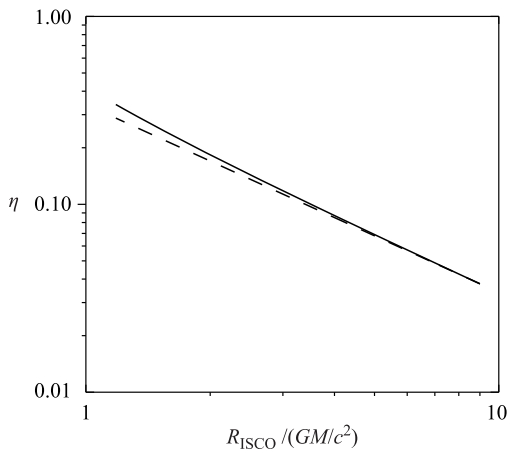

Fig. 17 The solid line shows numerical curve of the radiative efficiency η as a function of $R_{\rm ISCO}$. The dashed line shows $\eta \sim 1/R_{\rm ISCO}$, which approximates the numerical curve.

4.1 The first black hole spin measurement with X-ray spectral continuum fitting

In 1997, I and my colleagues proposed a method of measuring the BH spin in BHXBs. It started when we tried to measure the mass of the BH in GRO J1655–40 [11] by measuring $r_{\rm in}$ from its X-ray continuum spectral fitting and assuming the BH is not spinning; we found the mass of the BH is around $4M_\odot$ [79]. Coincidentally just when this paper was going to press, Orosz and Bailyn [80] announced their accurate measurement of the BH mass of GRO J1655–40, which is significantly larger than what we found. A co-author of our paper, Rashid Sunyaev urged me to resolve this apparent discrepancy. I immediately realized that a spinning BH of $7M_\odot$ in GRO J1655–40 would be consistent with the inferred with X-ray data, and added a note in proof in the paper suggesting this possibility [79]. This turns out to be the first BH spin measurement on record. I then invited two of my close friends and collaborators, Wei Cui and Wan Chen, to join me to apply this method systematically to other BHXBs; a new main conclusion in this work was that the first microquasar in the Milky Way, GRS 1915+105, also contains a spinning BH [47].

At the time DISKBB was the only available fitting model in the XSPEC package for determining $r_{\rm in}$ from an observed X-ray continuum spectra, if the disk continuum is described by the SSD model: $L_{\rm disk} = 4\pi\sigma r_{\rm in}^2 T_{\rm in}^2$, where $T_{\rm in}$ in DISKBB is the disk temperature at $r_{\rm in}$ (i.e., the peak disk temperature in SSD) and $L_{\rm disk}$ can be calculated from the disk flux (after the correction to absorption), the distance to the source and disk inclination (an issue to be discussed later). To determine the physical inner disk radius from the DISKBB parameter $r_{\rm in}$, several effects must be considered: i) electron scattering in the disk modifies the observed X-ray spectrum; ii) the temperature distribution in the disk is not accurately described by the Newtonian gravity as assumed in SSD; iii) the observed temperature distribution is different from the locally emitted one; iv) the observed flux is different from the locally emitted one. The latter three are all due to GR effects [52]. For each of the above effects, we introduced a correction factor, using the best available knowledge at the time. Since then, several improvements have been made to correct for these effects and this continuum fitting (CF) method is now quite mature in making accurate BH spin measurements, given sufficiently high quality X-ray continuum spectral measurements and accurate system parameters of the observed BHXB.

4.2 Further developments and applications of the continuum fitting method

This CF method of measuring BH spin has since been applied widely to essentially every BHXB with a well measured X-ray continuum spectrum showing a prominent thermal accretion disk component. In particular, this method has been improved and incorporated into the widely used X-ray spectral fitting package XSPEC, e.g., KERRBB [81], BHSPEC [82], and KERRBB2 [35, 37]. Both the KERRBB and BHSPEC are relativistic models, but they have their own drawbacks and advantages (See Ref. [35] for a detailed comparison). KERRBB includes all the relativistic effects, but it requires to fix the spectral hardening factor. In contrast, BHSPEC could calculate the spectral hardening factor on its own; however, it does not include the re-

turning radiation effect, which turns out to be an important factor in BH spin determination in BHXBs. KERRBB2 combines both models by generating the spectral hardening factor table from BHSPEC and using the table as the input for KERRBB. The research group led by Ramesh Narayan of Harvard University, Jeffrey McClintock at Smithsonian Astronomical Observatory (SAO), and Ronald Remillard of Massachusetts Institute of Technology (MIT) [83] has since applied this method and contributed to most of the BH spin measurements available in the community, as shown in Table 2.

The CF method relies on two fundamental assumptions: i) The measured $r_{\rm in}$ is uniquely related to $R_{\rm ISCO}$ of the BH. ii) There is no or negligible X-ray radiation from the plunging matter onto the BH beyond $R_{\rm ISCO}$. The latter has been studied with numerical simulations that include the full physics of the magnetized flow, which predict that a small fraction of the disk's total luminosity emanates from the plunging region [84]. However, in the context of BH spin estimation, it has been found that the neglected inner light in the CF method only has a modest effect, i.e., this bias is less than typical observational systematic errors [85, 86].

The first assumption above requires that the measured $r_{\rm in}$ remains stable as a BHXB changes its spectral state and luminosity. However it was noticed that $r_{\rm in}$ measured is usually much smaller, sometimes even smaller than $R_{\rm ISCO}$ of a extreme Kerr BH in a prograde orbit, when the X-ray spectrum contains a significant hard PL component, which is believed to be produced by inverse Compton scattering of the thermal disk photons in a hot corona. We realized that the inferred smaller $r_{\rm in}$ could be due to the lost thermal disk photons in the scattering process. We then investigated this problem and confirmed that the inferred $r_{\rm in}$ can be made consistent with $r_{\rm in}$ inferred from the thermal disk component dominated spectrum, if the scattered photons are recovered properly by doing detailed radiative transfer in the corona [65]; the same conclusion was also reached by the Harvard/SAO/MIT group independently without knowing our much earlier results [87]. Therefore the method of BH spin measurement by X-ray continuum fitting can also be applied to some SPL state with strong PL component. The stable nature of the measured $r_{\rm in}$ is proven with the textbook case of LMC X–3, when its X-ray luminosity varied over more than one order of magnitude observed in nearly two decades with many different X-ray instruments, as shown in Fig. 18 [88].

However, when ordered by the observed disk luminosity $l_{\rm D} = L_{\rm disk}/L_{\rm Edd}$, the measured $r_{\rm in}$ shows a clear increasing trend when $l_{\rm D} > 0.3$, as shown in Fig. 19 [88]. The similar trend has also been found in another BHXB

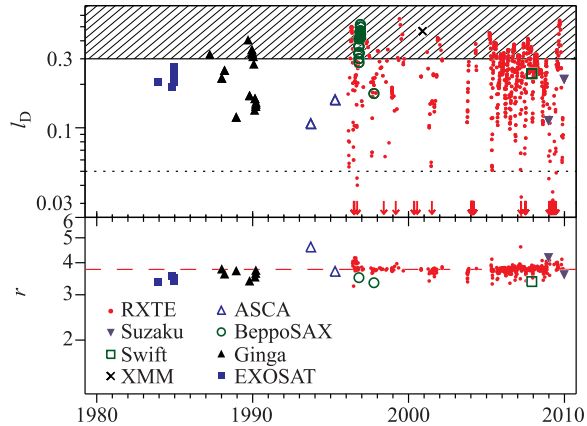

Fig. 18 The measured $r = r_{\rm in}/r_{\rm g}$ and disk luminosity $l_{\rm D} = L_{\rm disk}/L_{\rm Edd}$ (assuming $M_{\rm BH} = 10M_{\odot}$) as functions of observation time, for the BHXB LMC X–3. Reproduced from Ref. [88].

GRS 1915+105 [35] and two NSXBs [64, 89]. It was found that $r = r_{\rm in}/r_{\rm g}$ indeed increases physically when $l_{\rm D} > 0.3$, by comparing the evolution of r as a function of $l_{\rm D}$ over a large range for several BHXBs and NSXBs. Using the blackbody surface emissions of the NSs in these NSXBs is critical in evaluating any possible disk thickening due to high luminosity that would block at least part of the NS surface emission, as well as determining the actual NS mass accretion rate, which turns out to be much less than the disk mass accretion rate; this suggests that the increased radiation pressure is responsible for the increase of r and significant outflow when $l_{\rm D} > 0.3$ [64]. The same trend is much more pronounced in the super-Eddington accreting ultra-luminous X-ray source NGC1313 X–2, as shown in Fig. 20 together with the data from other BHXBs and NSXBs [90]. However the exact value of r obtained this way should be taken with caution, since the non-negligible energy advection at high accretion rate can modify the disk structure in

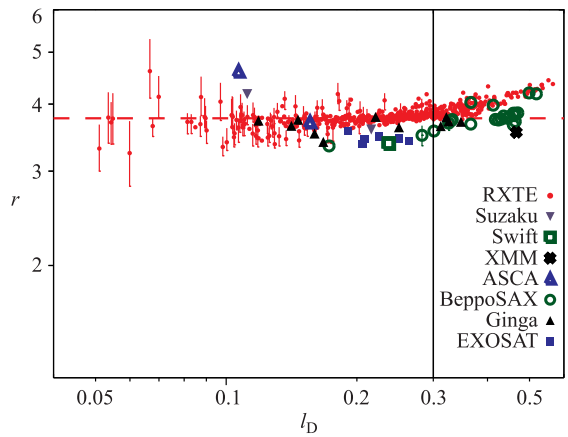

Fig. 19 The measured $r = r_{\rm in}/r_{\rm g}$ as a function of disk luminosity $l_{\rm D} = L_{\rm disk}/L_{\rm Edd}$ (assuming $M_{\rm BH} = 10M_{\odot}$), for the BHXB LMC X–3. Slightly adapted from Fig. 2 in Ref. [88].

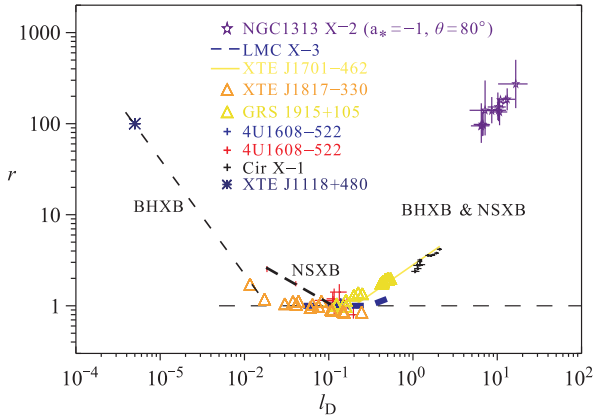

Fig. 20 The measured $r = r_{\rm in}/r_{\rm g}$ as a function of disk luminosity $l_{\rm D} = L_{\rm disk}/L_{\rm Edd}$, for several NSXBs and BHXBs, and the super-Eddington accreting ultra-luminous X-ray source NGC1313 X–2. All data points are taken from Ref. [64], except for that on XTE J1118+480 [93] and NGC1313 X–2 [90].

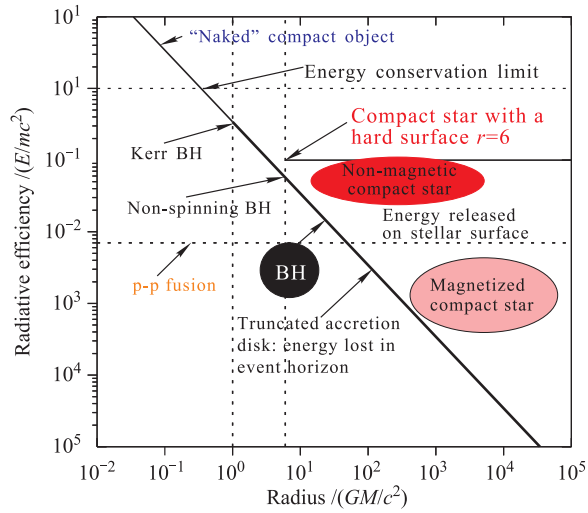

Fig. 21 The diagonal line shows a $1/r$ scaling, calibrated to take the value of 0.057 when $r = 6$. The thick black line is for a BH accreting systems. The range of $r = 1$–9 corresponds to the ISCO of a BH with different a_*; the radiative efficiency ranges between a few to several tens of percents, far exceeding the p-p fusion radiative efficiency taking place in the Sun. The case for $r > 9$ corresponds to TID, whose radiative efficiency can be extremely low, because energy is lost into the event horizon of the BH. The thin solid black horizontal line is for the 10% efficiency when matter hits the surface of a neutron star where all gravitational energy is released as radiation. The thin solid black diagonal line above the point marked for "Kerr BH" is for a speculated "naked" compact object [5], whose surface radius is extremely small and thus the radiative efficiency can be extremely high. Reproduced from Ref. [5].

non-trivial ways, thus making the SSD prescription inaccurate in this case [91].

Figure 20 also shows that as $l_{\rm D}$ decreases, r again starts to increases. However r increases at higher $l_{\rm D}$ and with a different slope for a NSXB than for a BHXB, which can be naturally explained as due to the "propeller" effect of the interaction between the NS's magnetosphere and its accretion disk [92] and the "no-hair" of the BH [90]. Figure 21 shows the radiative efficiencies of various systems; BHXBs may have either higher or lower efficiencies than NSXBs, because a BH has neither solid surface nor magnetic field [5].

It is interesting to compare the BH spin results in our first paper [47] and the most recent literature for the same BHXBs as listed in Table 2: i) For GRS 1915+105, A0620–003 and LMC X–3, both results are fully consistent; ii) For GRO J1655–40, the original result points to an extreme Kerr BH ($a_* \sim 0.93$) [47], somewhat different from the most recent result of mildly spinning BH ($a_* = 0.65 - 0.75$) [32]. However, the original result was obtained using the BH mass of $7M_\odot$, about 10% larger than the currently best estimate that was used to obtain an updated BH spin in the most recent literature [32]. From Fig. 15, it can be seen that a_* would be decreased from 0.93 to 0.87, if the BH mass is decreased by about 10%; actually $a_* = 0.85$ is also allowed in the new estimate [32]; iii) For Cygnus X–1, our original conclusion that $a_* = 0.75$ in the high/soft state and $a_* = -0.75$ in the low/hard state was based on the assumption that $r_{\rm in}$ decreased by a factor of two when the source made a transition from its normal low/hard state to the unusual high/soft state [94]. However the more realistic constraint is that $r_{\rm in}$ changed by more than a factor of 1.8–3.2 during the state transition [94], which implies that a_* switched from $|a_*| > 0.85$, fully compatible with the latest result of $a_* > 0.95$ in the high/soft state [37].

The above would suggest that a very low temperature disk component exists in its hard state spectrum, if Cygnus X–1 indeed harbors a Kerr BH and the accretion disk switches from a retrograde mode to a prograde mode when it makes the hard-to-soft state transition. For a supermassive BH in the center of a galaxy, it is well understood that its mass is mostly gained through accretion in its AGN phase [95]. Therefore random accretion (between prograde and retrograde modes) tends to make its final BH spin close to zero, regardless its initial BH spin. For Cygnus X-1, its current BH mass of around 10–20 $M_\odot$ cannot be gained through post-formation accretion, since its observed average mass accretion rate $\dot{M} \sim 2 \times 10^{-9} M_\odot$ /yr and the age of its companion is much less that 10^8 yr; actually the age of the companion is estimated to range from 4.6 and 7.8 million years [96]. This means that its post-formation BH mass growth is much less than a fraction of its current mass and thus its current BH spin must be quite close to that at birth. Even if accreting at Eddington rate, to grow its BH spin from 0 and the final mass to be the current observed value, the timescale is around 3.1×10^7 yr and

the accreted mass is roughly 7.3 $M_\odot$ [37]. If its accretions alternates between prograde and retrograde modes, then its current BH spin should be even closer to its initial spin than that in low mass BHXBs that only stay in one accretion mode due to roche-lobe overflows. Therefore the current high BH spin in Cyg X–1 must be natal; this conclusion is also true for the other highly spinning BHs in other BHXBs [48].

In summary, BH spin in BHXBs can now be measured reliably with the CF method, when the luminosity of a BHXB is between ~ 0.02 and ~ 0.3 in Eddington unit and their system parameters are well-known *a prior*. The observed thermal disk spectrum can be modeled directly to obtain the BH spin with the available KERRBB2 model in XSPEC when the X-ray spectrum in dominated by this component, i.e., the source is in the thermal state. When a significant power-law component is present, the inverse Compton scattering process must be taken into account to recover the disk photons scattered into this PL component, with for example the SIMPL/SIMPLR model [37, 97] in XSPEC. Recently another way to measure BH spin using the outburst properties of BHXBs has been proposed [77], which is mentioned briefly in Section 8; however the effectiveness of this method needs to be tested.

4.3 Uncertainties of the continuum fitting method

In spite of the tremendous progress made so far on BH spin measurements in BHXBs, most of these BH spin measurements suffer from considerable uncertainties. Actually the major source of these uncertainties comes primarily from the uncertainties in their BH masses, accretion disk inclination angles, and distances. The accurate BH mass measurement is required because $R_{\rm ISCO}$ must be in units of $r_{\rm g} = GM/c^2$ in Fig. 15. The disk inclination angle and distance are also required because the total luminosity of the disk emission $L_{\rm disk}$ is needed, in order to estimate the absolute value of a_*.

So far, all BH masses in X-ray binaries (XRBs) have been estimated using the Kepler's 3rd law of stellar motion, expressed in the so-called the mass function given in Eq. (1). Since the only direct observables are $P_{\rm orb}$ and $K_{\rm C}$, both $M_{\rm C}$ and i have to be determined indirectly in order to obtain the BH mass estimate reliably. The companion's mass $M_{\rm C}$ can be determined relatively reliably by the observed spectral type of the companion star and i can be estimated by modeling the observed ellipsoidal modulation of the companion's optical or infrared light curve. The observed ellipsoidal modulation is a consequence of exposing different parts of the pear-shaped companion star to the observer at different orbital phases (see Figs. 1 and 5); the pear-shape is caused by the tidal force of the compact star, which also heats the side of the companion star facing it. For details of BH mass estimates using this method, please refer to Ref. [2].

However, model dependence and other uncertainties (such as accretion disk contamination) cannot be circumvented completely and thus systematic error may exist in determining their system parameters. For example, three optical states, namely "passive", "loop" and "active" states, have been identified in the normally called "quiescent" state of A0620–003 when its X-ray luminosity is very low; only during the passive state its optical light curve modulation is purely ellipsoidal, i.e., accretion disk contamination is completely negligible, as shown in Fig. 22 [98]. This means that considerable systematic errors in determining its inclination angle may occur unless only the "passive" state data are used. Unfortunately previous observations of BHXBs used to determine their inclinations did not always occur during the passive state, thus systematic errors may be common in previous results [99]. Even for GRO J1655–40, of which all previous observations were made during its passive state [99], its BH mass measured with different observations, or the same data analyzed by different groups are not exactly the same, and even not completely consistent between them, as shown in Fig. 23, which show a scatter of about 20%–30% to the estimated BH mass, much larger than its statistical error of a few percents.

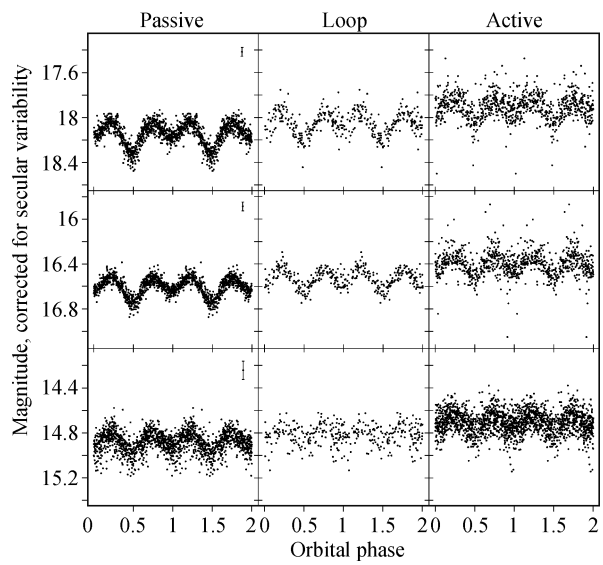

Fig. 22 Phased VIH ellipsoidal light curves corresponding to the three states, namely "passive", "loop" and "active" states; the data in each state and each wave band are plotted twice for clarity. Typical differential photometric error bars are shown in the upper right corner of the passive-state light curve for each band. To produce purer ellipsoidal light curves, variability on timescales greater than 10 days has been removed from loop- and active-state data. Reproduced from Ref. [98].

It should be pointed out that the inclination i in Eq. (1) refers to that of the orbital plane of the binary system. Because the accreting material initially carries the angular momentum inherited from the companion star, the formed disk should be co-planar with the orbital plane of the binary system. However, the BH spin in a BHXB cannot be changed significantly by accretion [71] (and see discussion above on Cygnus X–1). Therefore its spin axis may not coincide with the normal direction of the orbital plane of the binary system. In this case the Bardeen-Petterson effect [106], due to frame-dragging by the spinning BH, can rapidly align the normal axis of the inner disk region with the spin axis of the BH, making the inner disk and binary system mis-aligned. Circumstantial evidence already exists for mis-alignment between the two axes, because the orbital inclination of GRO J1655–40 shown in the upper panel of Fig. 23 is significantly different from $\sim 80°$ inferred from its relativistic jets [107], if the jets are powered by extracting the spin energy of the BH via the Blandford–Znajek mechanism [76]. Nevertheless, the orbital inclination is normally used in

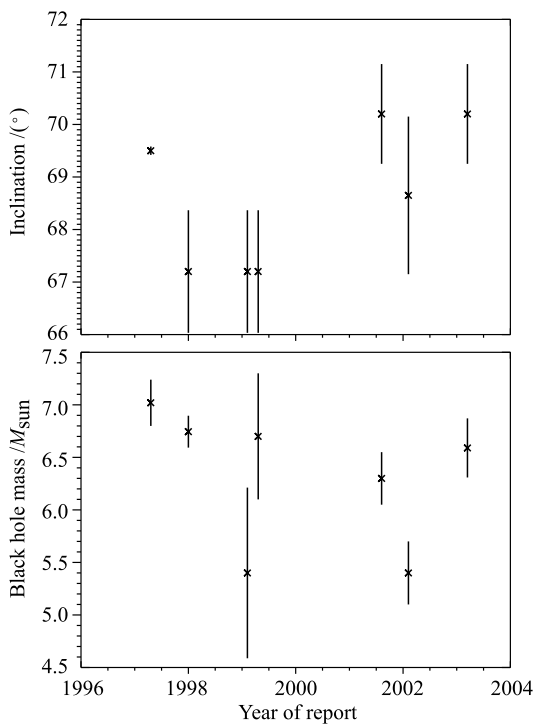

Fig. 23 The BH mass and system inclination of GRO J1655–40 reported at different times, ordered by their publication dates [80, 100–105]. Note that the third and fourth reports [101, 102] adopted the inclination in the second report [100], and the last (seventh) report [105] adopted the inclination in the fifth report [103].

place of the disk inclination, which is needed in BH spin measurement using the CF method, in order to infer the total disk luminosity and calculate GR correction factors. However, the inner disk inclination is currently not available essentially for any of the known BHXBs. For example, a mis-alignment of 10° from $i = 70°$ can cause nearly 50% error to the total disk luminosity, which will translate into nearly 30% error in $r_{\rm in}$. A Schwarzschild BH may be estimated to have a_* falling any where between $[-0.5, 0.5]$, if $r_{\rm in}$ is uncertain within about 30%, according to Fig. 15.

Accurate determinations of distances of astrophysical objects in the Milky Way are difficult, e.g., for BHXBs that are not standard candles. Normally some absorption features in their spectra, in conjunction with their positions in the galactic coordinates, are used to infer their distances. For example, the distance of GRO J1655–40 is commonly taken as 3.2 ± 0.2 kpc, based primarily on observed absorption lines and somewhat on the dynamics of the observed jets. Critical examinations of all available data related to its distance, however, are in favor of a much closer distance of less than 2 kpc and more likely just 1 kpc [108, 109]. Similar conclusion is also reached to the distance of A0620–003, revising its distance from the commonly accepted 1.2 ± 0.4 kpc to ~ 0.4 kpc, making its possibly the closest BHXB known so far [109]; however, a distance of 1.06 ± 0.12 pc was preferred in a more recent study [30]. Similarly the currently adopted distances of many other BHXBs may also have considerable systematic errors. If true, this would change significantly the current estimates on their masses and spins.

Therefore future improvements of the continuum fitting method depend upon the improved measurements on their BH masses, accretion disk inclination, and distances.

4.4 Future improvements of the continuum fitting method

The mass ratio q can be determined directly according to the law of momentum conservation, i.e.,

$$M_{\rm C}/M_{\rm BH} = K_{\rm BH}/K_{\rm C} \tag{1}$$

if the semi–amplitude of the velocity curve of the BH $K_{\rm BH}$ can be observed directly, as illustrated in Fig. 1. The orbital inclination i can be then calculated using Eq. (1), avoiding any systematics related to the ellipsoidal light curve modeling.

Since a BH is not directly observable, we can only hope to observe any emission or absorption line feature co-moving with it. The accretion disk certainly moves with the accreting BH. However any line feature of the inner accretion disk suffers from the broadening of disk's orbital motion and distortions by relativistic effects around the BH, thus making it practically impossible, or difficult at least, for detecting the binary orbital motion of

the BH. Orbital motion of double-peaked disk emission lines were observed for NSXB Sco X–1 [110], the BHXBs A0620–003 [111, 112] and GRS 1124–68 [112]. Unfortunately a significant phase offset of velocity modulation was found from that expected based on the observed orbital motion of the companion, though the velocity semi-amplitude is consistent with the expected mass ratio [112]. Soria *et al.* observed the orbital motion of the double-peaked disk emission line He II λ4686 from GRO J1655–40, and found its velocity modulation phase and semi-amplitude in agreement with the kinematic and dynamical parameters of the system [113]. However one major problem in accurately measuring the orbital motion of the primary from the observed double-peaked emission lines is how to determine reliably the line center, because the lines are typically asymmetric and also variable.

We have recently proposed to observe the Doppler shifts of the absorption lines of the accretion disk winds co-rotating with the BH around its companion star [114], since in many XRBs accretion disk winds are ubiquitous and appear to be rather stable when observed (e.g., in Ref. [115]). We verified this method using *Chandra* and *HST* high resolution spectroscopic observations of GRO J1655–40 (shown in Fig. 24) and LMC X–3. Unfortunately the currently available data only covered small portions of their orbital phases and thus do not allow better constraints to their system parameters. Future more observations of these two sources and other sources with detectable absorption lines from their accretion disk winds will allow reliable and precise measurements of the BH masses and orbital inclination angles in accreting BHXBs.

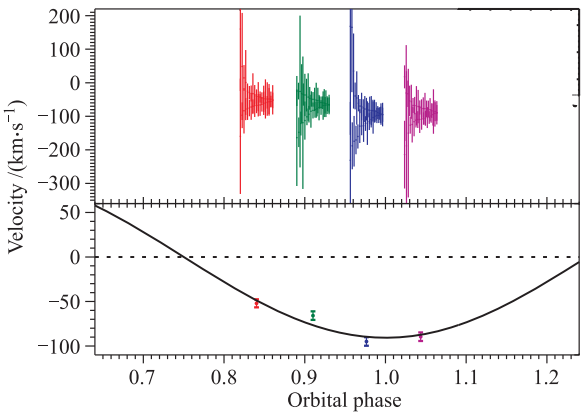

Fig. 24 Velocity curve of the 39 observed X-ray absorption lines with *Chandra* from GRO J1655–40, after subtracting the line of sight intrinsic velocity of each line at each orbital phase. The upper panel marks the velocity of each line with its 1–σ error bar, slightly shifted horizontally for visual clarity. The bottom panel shows the weighted average velocity of all lines in the upper panel at each phase; the solid curve is the fitted velocity curve with its orbital period and phase fixed at the values observed previously. Reproduced from Ref. [114].

Since the accretion disk has very high density and is ionized near the BH, where the majority of the observed disk emission is produced due to the very deep gravitational potential near the BH, scattering of the primary disk emission is inevitable. The scattered light is polarized and its polarization fraction and position angle depend on the viewing direction (inclination), scattering optical depth and the radius where the scattering occurs 116–119. Ignoring many details, it can be shown that the polarization fraction, $P(i)$, of the observed disk photons (initial disk emission plus the scattered emission) is given by

$$\frac{1}{P(i)} = 1 + A\frac{\cos i}{1-\cos^2 i} \tag{5}$$

where A is a constant depending upon the scattering optical depth; detailed calculations made by Chandrasekhar [120] gives $P(75°) = 0.04$. Note that here the disk photons are from the Raleigh–Jeans part of the multi-color blackbody spectrum with a characteristic shape of $f(\nu) \propto \nu^{1/3}$, i.e., no GR effect is included. We can therefore find the disk inclination angle by measuring the polarization fraction of this part of the disk emission, as shown in Fig. 25. At energies above the Raleigh–Jeans part of the multi-color blackbody spectrum, the polarization is strongly effected by both the inclination and BH spin, as shown in Fig. 26. The continuum spectra are clearly degenerated for the different combinations of inclination and BH spin, but the polarization fraction and angle as functions of energy can clearly distinguish between them [118]. Therefore X-ray spectra-polarimetry observations of BHXBs will certainly make important progresses in measuring BH spin.

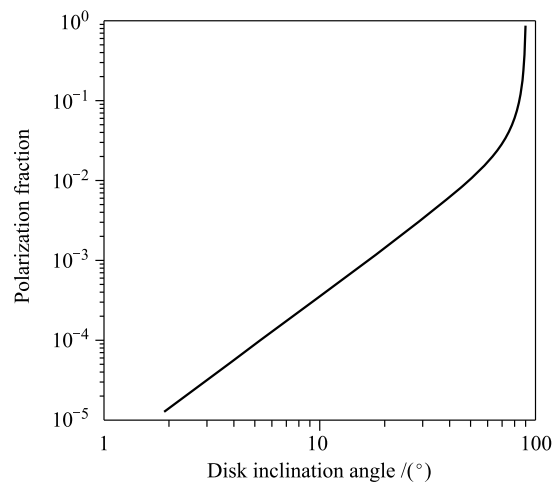

Fig. 25 Polarization fraction of observed accretion disk emission as a function of its inclination.

Besides using polarization measurements to obtain inner disk inclination (and BH spin), the broad iron

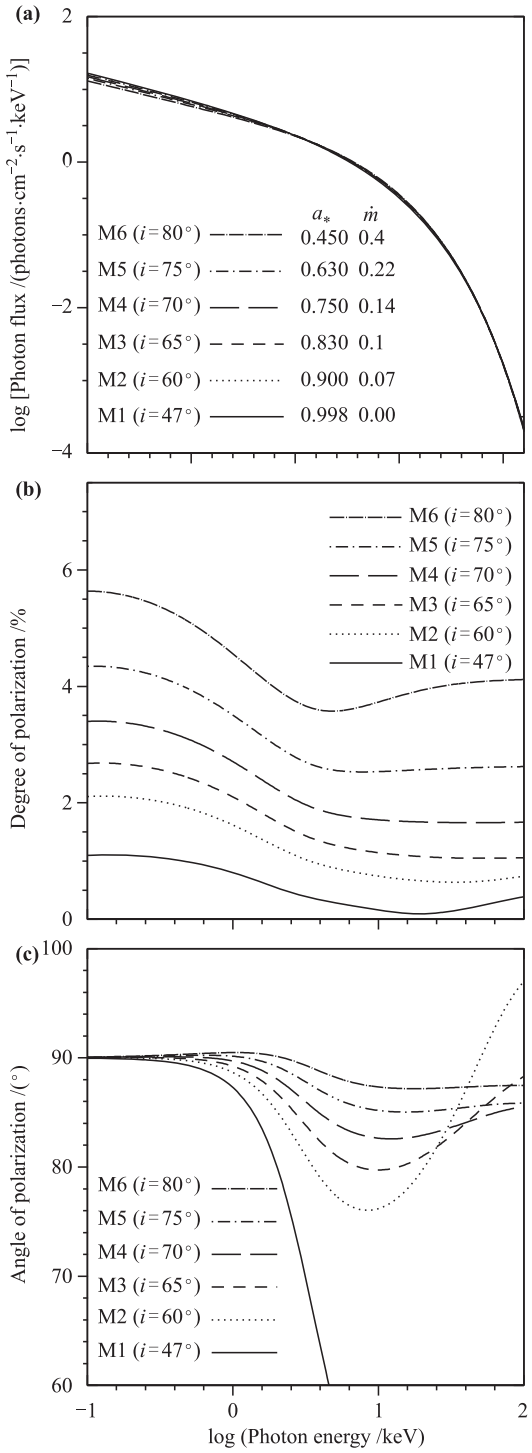

Fig. 26 Disk continuum flux **(a)**, polarization fraction **(b)** and polarization angle **(c)** as functions of photon energy for different model parameters. i, inclination angle of the inner disk in degrees; $\dot{m}$, mass accretion rate in units of Eddington rate by assuming a 10% conversion efficiency from rest mass to radiation in all cases. Other parameters: mass of the BH is $10M_{\odot}$; distance to the BH is 10 kpc; spectral hardening factor is 1.6. Reproduced from Ref. [118].

K-alpha measurements can also be used to do so [121–123], because iron K-alpha emission is believed to come from the fluorescent emission of the disk as a result of illumination by a hard X-ray source above the disk. Naturally this emission is sensitive to the disk inclination (and BH spin). However, compared to the polarization measurement method, this method is less straight forward and may suffer from systematic uncertainties in deriving the disk inclination (and BH spin), because complicated modeling of the hard X-ray component and line emissivity from the disk is required. Therefore it is essential to use all methods discussed above to measure both inclination angles (orbital plane and inner disk) and BH spin. Studying the relationship between the results obtained with different methods is also important in its own rights, in order to understand accretion disk physics, its interaction with the BH in its center, production of relativistic jets, the origin of the BH spin, and ultimately the formation mechanisms of BHs and BHXB systems.

The recent dispute on the distances of GRO J1655-40 and A0620–003 exemplifies the difficulty of determining the distances of BHXBs using mostly absorption lines [108, 109]. We have recently suggested a method of using the delay time between the X-ray fluxes of an XRB and its X-ray scattering halo by interstellar dust to infer its distance [124, 125]. However this method may suffer from our incomplete knowledge of the distribution of interstellar medium. Ideally precise astrometry can determine their distances model-independently, by measuring their trigonometric parallaxes. Recently the distance to Cygnus X–1 was determined reliably and accurately this way ($1.86^{+0.12}_{-0.11}$ kpc; [126]); which is key to the consequent measurement of its BH mass and spin [36, 37]. Currently it remains challenging to measure the trigonometric parallaxes of objects at distances beyond several kpc where most BHXBs are located. Future high precision astrometry missions are expected to improve the distance estimates to these BHXBs significantly.

Therefore we expect that the improved measurements discussed above on their BH masses, inner disk inclination, and distances will allow future improvements of BH spin measurement with the CF method.

4.5 Possible application of the continuum fitting method to AGNs

More recently, the CF method is also applied to constrain the BH spin in an active galactic nucleus (AGN), which is powered by matter accretion onto the central supermassive BH in its center [127]. However the BH spin inferred this way for an supermassive BH is quite uncertain, because: i) The peak temperature of the accretion disk inversely increases with the mass of a BH. Therefore, for a supermassive, its temperature would be

in the ultraviolet energy range which will be strongly absorbed and hard to observe; ii) The system parameters of a supermassive BH (e.g., the mass of the BH and the inclination angle of the accretion disk) have larger uncertainties; iii) The uncertain mechanism for some components (e.g., the soft X-ray excess) in AGN spectra also increases the difficulty; iv) Some emission and absorption lines may distort the continuum spectrum substantially; and v) In some cases the contribution of its host galaxy to the observed total continuum spectrum cannot be removed satisfactorily.

The polarized continuum of an AGN should be a pure accretion disk continuum, at least in the optical to near infrared band [128]. One possible way to measure the BH spin in an AGN with the CF method is to combine the observed polarized optical to near infrared continuum spectrum with the observed total UV continuum spectrum to get a broad band continuum spectrum of an AGN [129]. In principle the broadened Balmer edge features and the total UV spectrum can be used to constrain the disk inclination angle and fraction of host galaxy contamination, respectively [129]. However the quality of the currently available data is still insufficient to allow accurate determination of BH spin in AGNs with this method.

Nevertheless the principal method of measuring BH spin in AGNs should be using the reflected broad iron line and continuum components [121–123]. The main reason is that i can also be determined simultaneously and $r_{\rm in}$ obtained this way is already in units of $r_{\rm g}$, thus avoiding naturally the uncertainties caused by the BH mass and inclination in the CF method. However cross calibration can be done between the CF and reflection fitting methods if both can be applied to the same supermassive BH.

5 Further developments on hot accretion flows

In this section I briefly summarize some further developments on hot accretion flows, which are believed to be responsible for the PL component of the spectra in BHXBs. The multi-waveband spectra of the hard state of the BHXB XTE J1118+480 was modeled with the TID with hot accretion flow (ADAF) geometry [panel (a) in Fig. 27] and TID (with ADAF) plus jet model [panel (b) in Fig. 27], with $\dot{m}_{\rm D} = 0.05$ and $\dot{m}_{\rm jet} = 5 \times 10^{-3}\dot{m}_{\rm D}$ [93]. The steep UV spectrum provides clear evidence for a large truncation radius for the SSD ($r = 600$), and the radio to infrared spectrum dominates the jet emission, which also contribute to the hard PL component

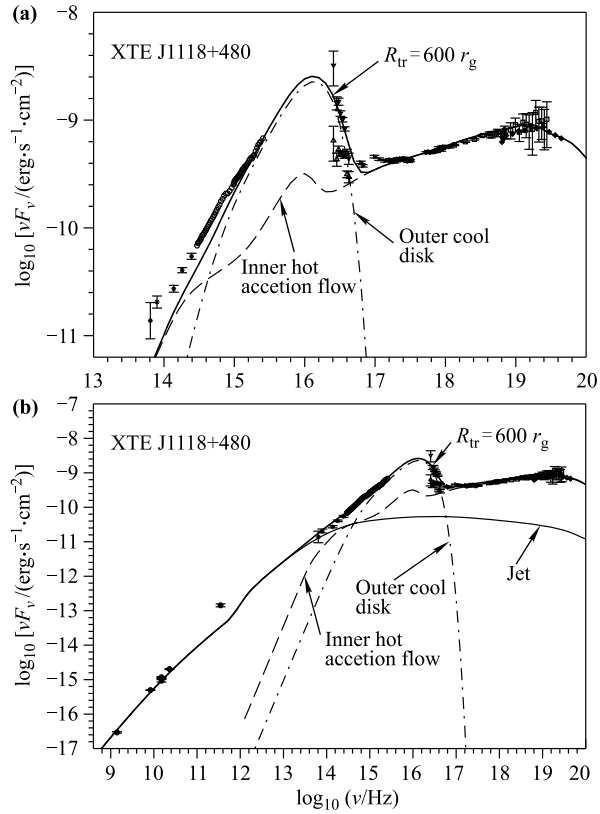

Fig. 27 Spectral modeling results for XTE J1118+480. **(a)** Outer cool disk plus inner hot accretion flow model. **(b)** An additional jet component is included. $\dot{m}_{\rm D} = 0.05$ and $\dot{m}_{\rm jet} = 5 \times 10^{-3}\dot{m}_{\rm D}$. Reproduced from Ref. [93].

[93]. Such low accretion rate gives very low SSD luminosity $l_{\rm D} \sim 5 \times 10^{-4}$ (since the disk radiation efficiency $\eta \sim 1/r$; see Fig. 17), which is far below the turn-over luminosity of $l_{\rm D} \sim 10^{-2}$ shown in Fig. 20. Therefore the inferred truncation radius of XTE J1118+480 agrees with the extrapolation of data points of XTE J1817–330 down to very low disk luminosity. Large truncation radii are also reported from several other sources in the hard state (e.g., in Ref. [130]). However, the exact values of these truncation radii may have large uncertainties, since no direct detection of the inner disk peak emission was available, unlike the strong case of XTE J1118+480 [93]. For this reason I did not include these reported values in Fig. 20.

Panel (b) in Fig. 27 also shows that the radiation from both the hot accretion flow and the jet contribute to the X-ray emission. However the former is roughly proportional to $\dot{m}^2$, whereas the latter to $\dot{m}$. Thus with the decrease of $\dot{m}$, the contribution from the jet becomes more and more important, thus the X-ray radiation will be dominated by the jet (when $l \lesssim 10^{-5}$–10^{-6}), as shown in Fig. 28 [93]. The observational data of very low-luminosity AGNs clearly show a correlation between

radio and X-ray with a correlation index of ~ 1.2 [131], in excellent agreement with the prediction shown in Fig. 28 [93].

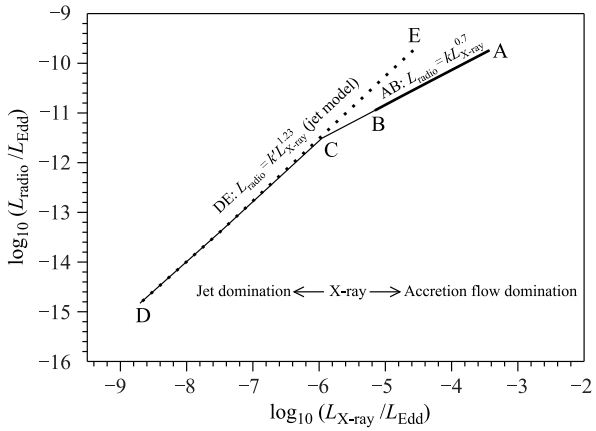

Fig. 28 Radio (8.6 GHz) – X-ray (2–11 keV) correlation for BHXBs. The observed correlation is shown by the segment AB. Segments BCD show the predicted correlation at lower luminosities, which approaches that of a pure-jet model, as shown by the segment DE. Note that below the point $C(\sim 10^{-6} l_{\rm D})$, the X-ray emission is dominated by the jet and the correlation steepens. Reproduced from Ref. [132].

It is well known that the highest luminosity an ADAF can produce is only about $3\% L_{\rm Edd}$. However the observed highest luminosity a hard state can reach can be $10\% L_{\rm Edd}$ or even higher, which can be described by LHAF shown in Fig. 29, where several previously known solutions of accretion flows are all unified in a single scheme [133]. The hard state spectrum of XTE J1550–564 with $L \sim 6\% L_{\rm Edd}$ is explained by LHAF very well, including the X-ray spectral slope and the value of the cutoff energy [134].

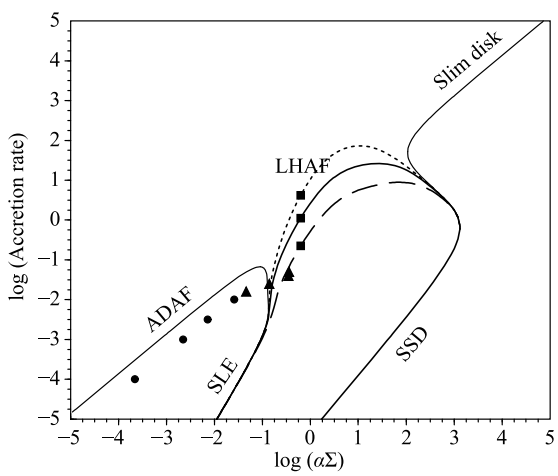

Fig. 29 The thermal equilibrium curve of various accretion solutions. The accretion rate is in units of $\dot{M}_{\rm Edd} \equiv 10 L_{\rm Edd}/c^2$ and the unit of Σ is g·cm^{-2}. The parameters are $M_{\rm BH} = 10 M_\odot, \alpha = 0.1$, and $r = 10$. Reproduced from Ref. [133].

6 Further developments on corona formation

While the formation of the SSD in a BHXB is reasonably well understood, the formation of the corona, which is the hot accretion flow discussed in Section 5, remains less understood. Over the last more than 10 years, Liu and her collaborators have developed a model to explain the formation and evolution of the corona in a BHXB or AGN, in which the mass accretion rate $\dot{m}$ in units of the Eddington ratio drives the variations of the complex accretion flows by the interaction between the cold SSD and the hot corona [60, 135–139]. Specifically, the coupling between the hot corona and the cold disk leads to mass exchange between them. The gas in the thin disk is heated up and evaporates into the corona as a consequence of thermal conduction from the hot corona, or the corona gas condenses into the disk as a result of overcooling by, for example, external inverse Compton scattering. If $\dot{m}$ is low, evaporation occurs and can completely remove the thin disk, leaving only the hot corona in the inner region and a truncated thin disk in outer region; this provides a mechanism for ADAF at low $\dot{m}$. If $\dot{m}$ is high, the gas in the corona partially condenses to the disk due to strong Compton cooling, resulting in disk dominant accretion. The model naturally explains the different structures of accretion flow in different spectral states as shown in Fig. 30 [60, 135, 137–144]. The hysteresis observed in spectral state transitions can also be explained by different irradiations from different evolution history under the same scenario [145–147].

Figure 30 is significantly different from the illustration of accretion flow structures in different spectral state in Fig. 12 on three aspects: i) At intermediate $\dot{m}$, the SSD is broken by ADAF into two parts, an outer disk and an inner disk; ii) The inner disk boundary here is always located very close to the BH, except in the very low $\dot{m}$ hard or quiescent state, which is very different from the TID scenario depicted in Fig. 12; iii) The corona here covers essentially the whole accretion disk, especially the inner disk region, whereas in Fig. 12 the corona is mostly located inward from the inner disk boundary. The observed soft X-ray component in the low/hard state can be explained by the existence of the inner disk [139, 140, 142, 144]. As I have discussed above, the inner disk boundary radius inferred with the CF method in the presence of a strong PL component is actually consistent with that in the soft state when the PL component is weak, after taking into account the Compton scattering in the corona [65, 87]. Actually the essential assumption behind the broad iron line/reflection fitting method of determining BH spin is that the inner disk boundary is at the ISCO

when the PL component is strong. All these tend to support the existence of the inner disk at intermediate $\dot{m}$. However it remains to be demonstrated that if the whole SSD is indeed broken into the two parts at intermediate $\dot{m}$, as illustrated in Fig. 30.

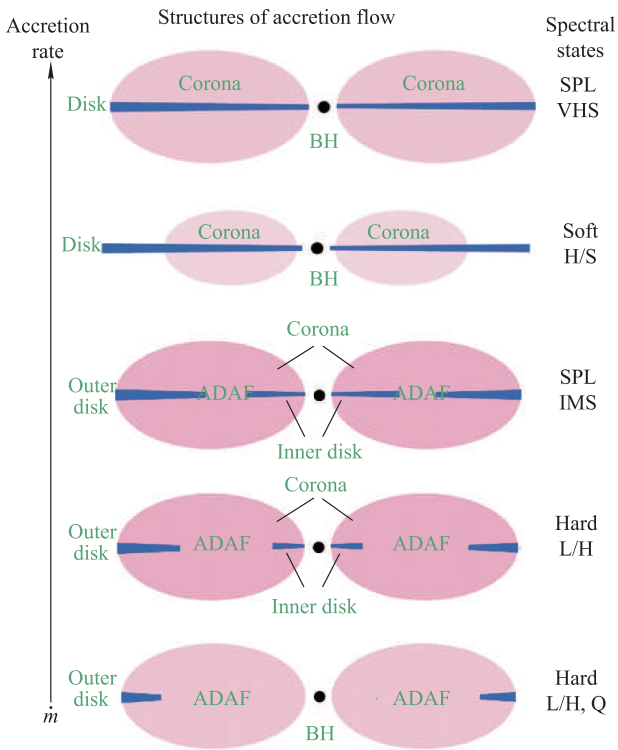

Fig. 30 A schematic description of the accretion flow structures in different spectral states as consequences of disk-corona interaction, which is primarily driven by mass accretion rate *dotm*. SPL: steep power-law state; VHS: very high state; Soft: soft state; H/S: high/soft state; Hard: hard state; L/H: low/hard state; Q: quiescent state. Adapted from a similar figure provided by Prof. Bifang Liu.

Recently it has been suggested that the ADAF and corona shown in Fig. 30 may have clumpy structures, as shown in Fig. 31 [148]. The "clumpy" model (Fig. 31) has mainly two different consequences from the "uniform" model (Fig. 30): i) The inner disk is transient in the "clumpy" model; ii) The "clumpy" model can explain the variabilities observed in X-ray binaries (such as the state transitions discussed in Section 7 and radio-loud AGNs (such as BL Lac objects).

Determining the structure of the corona in an BHXB observationally remains difficult; the fundamental issue on whether the corona covers mostly the accretion disk or the central compact object still remains unclear so far. Since the observed similar spectral and state transitions between some NS and BH XRBs are quite similar [149], it is reasonable to assume that they have similar coronae. Recently we have used type I X-ray bursts from low-mass

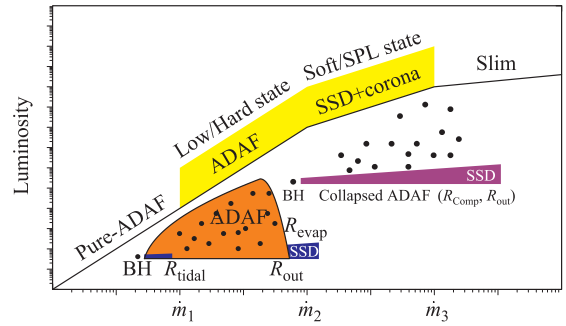

Fig. 31 *Solid lines*: accretion disk models at different accretion rates. Clumpy structures in either ADAF or corona (shown as insets) may be developed at intermediate accretion rates, corresponding to different spectral states. Reproduced from Ref. [148].

NSXBs to show that X-ray bursts experience negligible Comptonization and that the corona cools rapidly during the rising phase of X-ray bursts and is then heated up rapidly during the rising phase of X-ray bursts, as shown in the upper panel of Fig. 32 for IGR J1747–721 [150]. These results suggest that the corona cannot cover the central compact object completely (lower panel of Fig. 32) and that the destruction and formation time scales of the corona are as short as seconds; such short time scales are quite difficult to understand in the above discussed evaporation model, in which the time scales are related to the viscous time scales of the accretion disk. However, this short time scale is consistent with a corona produced by magnetic reconnections in the accretion disk, in a

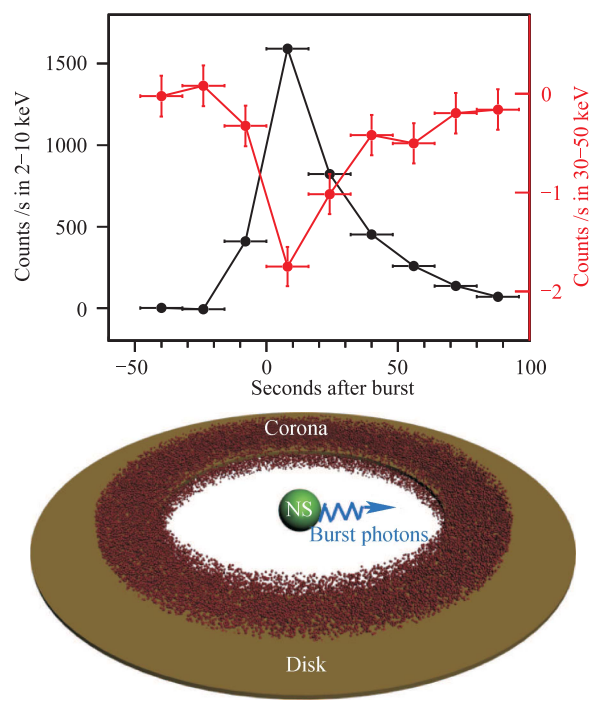

Fig. 32 *Upper panel*: Anti-correlation between the observed type I X-ray bursts from surface of the NS in IGR J1747–721 Reproduced from Ref. [150].

similar way to the solar corona heating [151]; this conclusion was based on the inferred accretion flow structure of a BHXB shown in panel (a) of Fig. 33, in comparison with the atmospheric structure of the Sun shown in panel (b) of Fig. 33.

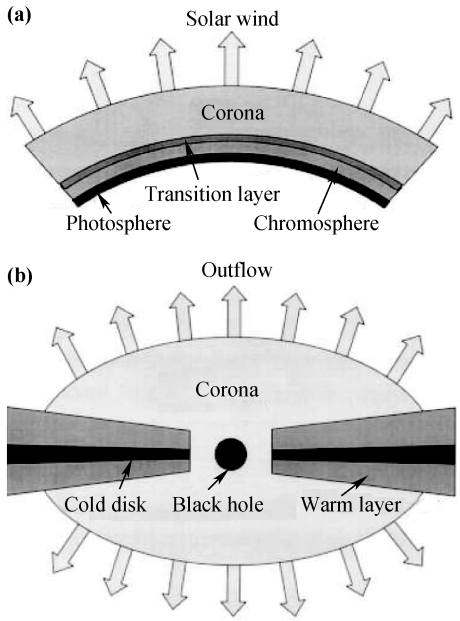

Fig. 33 Schematic diagrams of the solar atmosphere **(a)** and accretion disk structure **(b)**. Reproduced from Ref. [151].

It is worth noticing that the purported coronae in both XRBs and AGNs have strikingly similar properties, e.g., they all have electron temperatures of the order of hundreds keV, in spite that the temperatures, inner disk radii and variability time scales of their cold accretiondisks all scale with their BH masses (and accretion rates) as predicted in the SSD model. This means that their coronae are scale independent. It is perhaps not coincidental that the electrons' velocities in a corona are approximately the same as the Keplerian orbital velocities of the inner disk, which are also roughly the same as the launching velocities of jets. Of course these velocities are also the varialized velocities of the central BHs. It is plausible that turbulent small scale magnetic fields lifts the plasma in the "warm layer" shown in Fig. 33 to form the corona, which is then launched into the jets by the rotating large scale magnetic fields through either the BP or BZ mechanism; during these processes the magnetic fields are mostly responsible for changing the directions of motion of plasmas by the Lorentz force. If the corona is clumped as discussed in Section 6 [148], then the plasma channeled into the jets should be clumpy and thus the ejected jets should be episodic and have knotted structures, in agreement with observations; this scenario is illustrated in Fig. 34. Alternatively episodic ejections may also occur in the disk, similar to the coronal mass ejection on the Sun [152].

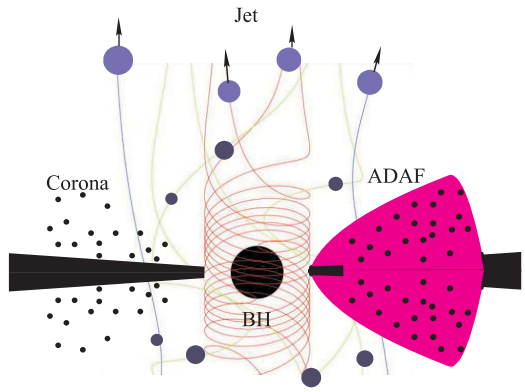

Fig. 34 The clumps in the clumpy corona/ADAF of a BHXB are channeled into the rotating and wound-up magnetic field lines and then ejected from the system. The launched jets should be episodic and have knotted structures.

Interestingly, the soft X-ray excess (SXE) frequently observed in AGNs can be interpreted as the warm layer found in XRBs, since the inferred plasmas parameters, with electron temperature of 0.1 to 0.3 keV and Compton scattering optical depth of around 10, are similar to that of XRBs and universal among AGNs with different BH masses, but seem to be related only with $\dot{m}$ [153–155]. Therefore their warm layers are also scale independent. Indeed, magnetic flares, perhaps caused by magnetic reconnections in the cold disk, can produce the warm layers in both XRBs and AGNs [156, 157].

7 Further developments on state transitions

To further understand the mechanism of the spectral state transitions, it is important to study those spectral state transitions in individual BHXBs during different outbursts. The advantages are obvious – uncertainties in our estimates of black hole mass, the binary properties such as the orbital period, or the source distance will not play any role in producing the observed diverse transition properties in individual BHXBs, which can only be driven by the accretion process under different initial conditions. The sources which firstly allowed such a study were the BH transients GX 339–4 and XTE J1550–564, the NS transient Aquila X–1, and the flaring NS low-mass XRB (LMXB) 4U 1705–44, in which a remarkable correlation between the luminosity of the hard-to-soft transition and the peak luminosity of the following soft state was found [158–160]. More recently, a comprehensive study of the hard-to-soft spectral state transitions detected in all the bright XRBs in a period of about five years with simultaneous X-ray monitoring

observations with the RXTE/ASM and the Swift/BAT confirmed the correlation between the hard-to-soft transition and the peak luminosity of the following soft state [161, 162], as shown in the upper panel of Fig. 35 [161]. More important was the discovery of the correlation between the transition luminosity and the rate-of-change of the luminosity during the rising phase of an outburst of transients or a flare of persistent sources, as shown in the lower panel of Fig. 35 [161].

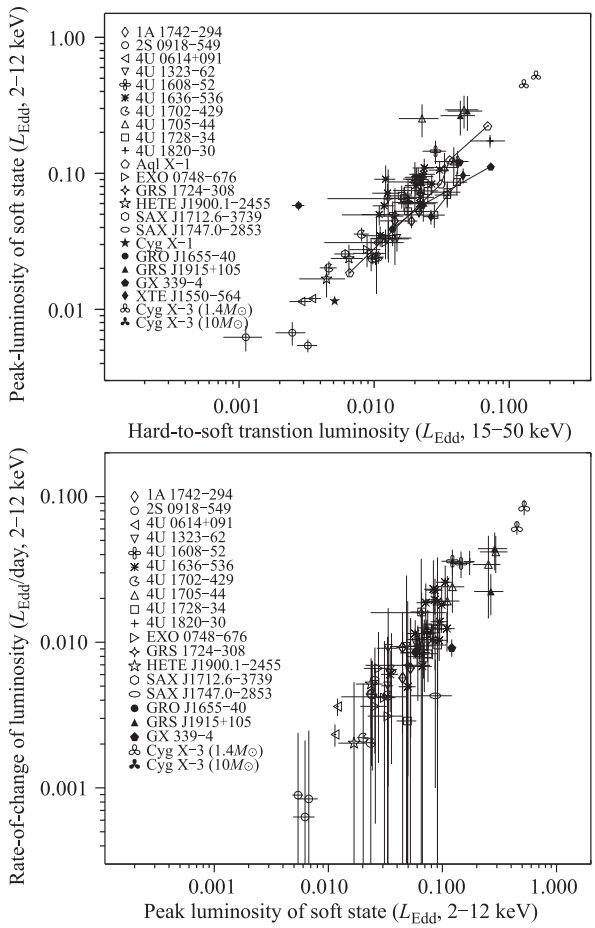

Fig. 35 *Upper panel*: Correlation between the transition luminosity (15–50 keV) and the peak luminosity of the following soft state (2–12 keV) in Eddington units. *Lower panel*: Correlation between the peak luminosity of the soft state and the maximum rate-of-increase of the X-ray luminosity around the hard-to-soft transition. Reproduced from Ref. [161].

The above correlation implies that in most cases it is the rate-of-increase of the mass accretion rate, rather than the mass accretion rate itself, determines the hard-to-soft spectral transition; this is depicted in Fig. 36 [161]. In addition, the discovery of the relation between the hard X-ray peak flux and the waiting time of transient outburst in the BH transient GX 339–4 (as shown in Fig. 37) supports that the total mass in the disk determines the peak soft state luminosity of the following outburst [159]. Therefore spectral states should be understood in the non-stationary accretion regime, which would be described by both $\dot{m}$ and $\ddot{m}$, as well as the total mass in the disk before an outburst.

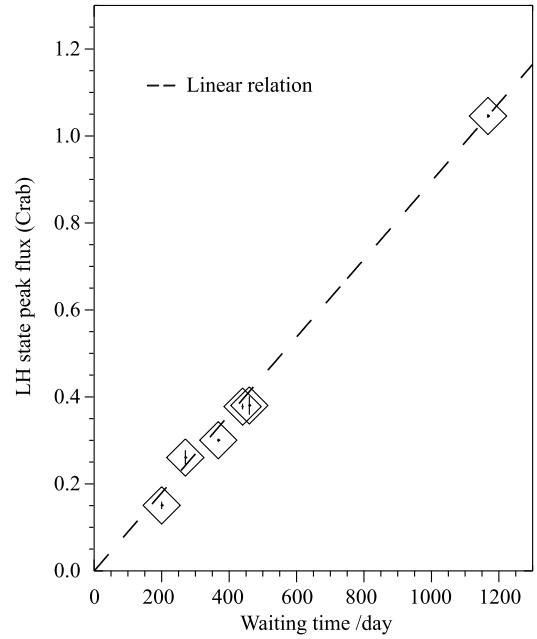

Fig. 36 Correlation between the peak fluxes of the initial low/hard states in the outbursts of GX 339–4 and the time since the latest low/hard state peak in the previous outburst. The dashed line passes the origin and the data point of maximal peak flux, showing an example of a linear relation. Reproduced from Ref. [159].

8 Further developments on thermal stability of SSD

The SSD model predicts that when the accretion rate is over a small fraction of the Eddington rate, which corresponds to $L \gtrsim 0.06L_{\rm Edd}$, the inner region of the disk is radiation-pressure-dominated and then both secularly [163] thermally unstable [164, 165]. However, observations of the high/soft state of black hole X-ray binaries with luminosity well within this regime ($0.01L_{\rm Edd} \lesssim L \lesssim 0.5L_{\rm Edd}$) indicate that the disk has very little variability, i.e., quite stable [166]. It has been well established that the accretion flow in this state is described by the SSD model [4, 167]. Radiation magnetohydrodynamic simulations of a vertically stratified shearing box have confirmed the absence of the thermal instability [168]. Recently, the thermal stability is revisited by linear analysis, by taking into account the role of magnetic field in the accretion flow [169]. By assuming that the field responds negatively to a positive temperature perturbation, it was found that the threshold of accretion rate above which the disk becomes thermally unstable

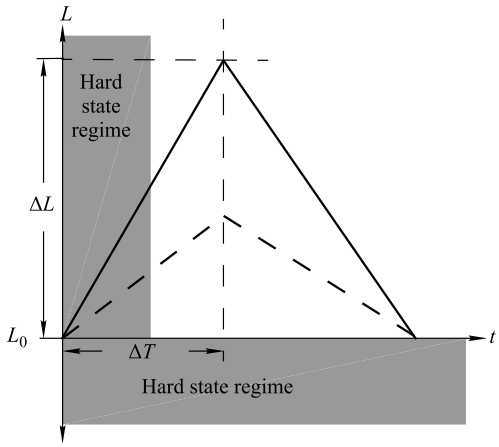

Fig. 37 A schematic picture of the regimes of the hard state. Two assumed transient outbursts of different peak luminosities are shown. When a source is under stationary accretion, spectral transitions between the hard state and the soft state occurs at a nearly a constant luminosity L_0. When a source is undergoing an outburst or flare, the hard-to-soft transition occurs at a luminosity above L_0. The additional luminosity roughly proportional to $\frac{\Delta L}{\Delta T}$. The soft-to-hard transitions are expected to occur around L_0. Reproduced from Ref. [161].

increases significantly, compared with the case of not considering the role of magnetic field. This accounts for the stability of the observed sources with high luminosities, as shown in Fig. 38. If the magnetic pressure is less than about 24% of the total pressure, then this model can explain the "heart-beat" limit-cycle instability observed in GRS 1915+105 at its highest luminosity; this peculiar source holds the highest accretion rate (or luminosity) among BHXBs.

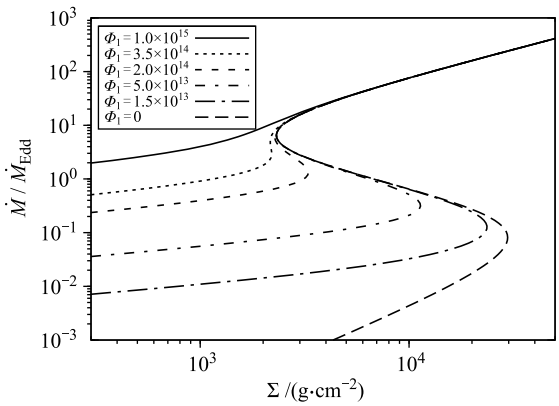

Fig. 38 The thermal equilibrium curves of a thin disk at $10r_g$ for different Φ_1, which is defined as $\Phi_1 \equiv B_\varphi H$ and is in unit of Gs·cm. Other model parameters are BH mass $M_{\rm BH} = 10M_\odot$ and viscosity parameter $\alpha = 0.1$. Reproduced from Ref. [169].

Observations of GRS 1915+105 showed that $t_{\rm high}$ (the duration of the outburst phase) is comparable to $t_{\rm low}$ (duration of the quiescent phase) and $L_{\rm high}$ is 3 to 20 times larger than $L_{\rm low}$ [170]. However, numerical calculations showed that $t_{\rm high}$ is less than 5 percent of $t_{\rm low}$, and $L_{\rm high}$ is around two orders of magnitude larger than $L_{\rm low}$. Some efforts have been made to improve the theory in order to explain observations either by some artificial viscosity prescription [171] or by additional assumption of the energy exchange between the disk and corona [172]. Taking into account the stress evolution process, it was found that the growth rate of thermally unstable modes can decrease significantly owing to the stress delay, which may help to understand the "heart-beat" limit-cycle variability of GRS 1915+105 [173]. The limit-cycle properties are found to be dominated by the mass-supply rate (accretion rate at the outer boundary) and the value of the α-viscosity parameter in the SSD model that assumes that the viscous torque is proportional to the total pressure [77]. It was also found that only the maximal outburst luminosity (in Eddington units) is positively correlated with the spin of a BH, providing another way to probe BH spin [77]; this is mainly due to the smaller inner disk radius and thus higher radiative efficiency for larger a_* as shown in Figs. 15, 16 and 17.

9 Unification and outlook

Despite of the many progresses made over the last

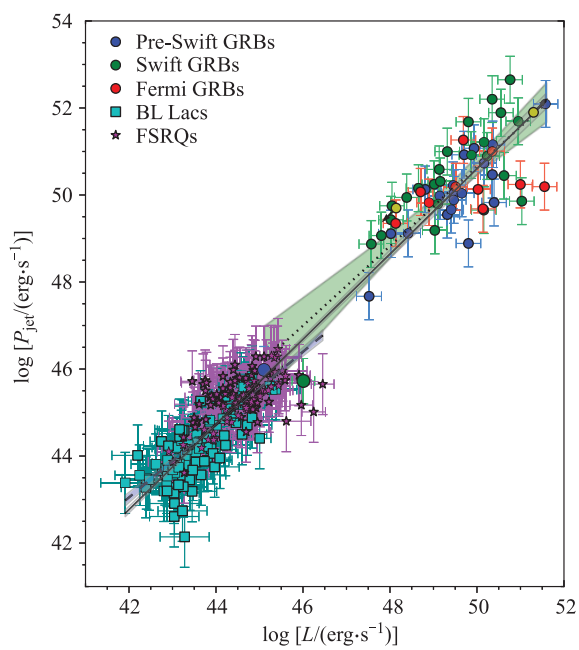

Fig. 39 The relation between the collimation-corrected gamma-ray luminosity and the kinetic power for AGNs and GRBs. The shaded regions display the 2σ confidence band of the fits. The blazar and GRB best-fit models (*dashed and dotted lines*, respectively) follow correlations which are consistent, within the uncertainties, with the best-fit model obtained from the joint data set (*solid line*). Reproduced from Ref. [175].

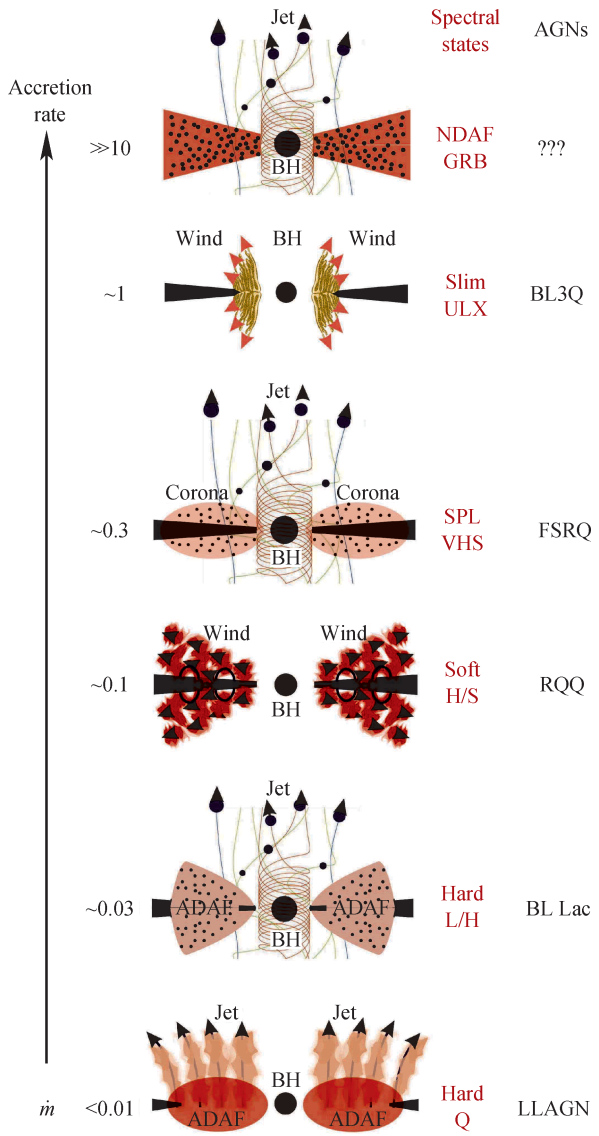

Some necessary elaborations and points:

- $\dot{m} \gg 10$: the two-phase clumpy thick disk is in the form of neutrino dominated accretion flow (NDAF), which can extend to ISCO due to the extremely low opacity of neutrinos. The large scale magnetic field lines are wound-up by the spinning BH and rotating disk. The discontinuous jet is produced by the BZ mechanism. Most likely no such ultra-Eddington AGN exists.
- $\dot{m} \sim 1$: the thin disk is truncated by radiation pressure, which drives near-spherical winds out. BL3Q is predicted as the early phase of a quasar, when the radiation pressure drives all gas in the radiation cone out so that no broad-line region (BLR) can be formed [179]. Actually all gas mixed with dust in the radiation cone can be blown out at substantially below Eddington rate, since the dust has a very high opacity to emissions from visible to UV. There BL3Q should be generic in the early phase of a quasar's active cycle, if the quasar activity is triggered by enhanced mass inflow consisting of a mixture of gas and dust.
- $\dot{m} \sim 0.3$: the thin disk extends to around ISCO and the two-phase corona is clumpy, so the jet is produced mostly via the BZ mechanism and is discontinuous. The dusty torus and BLR for in a FSRQ are not shown.
- $\dot{m} \sim 0.1$: the thin disk extends to around ISCO and near-equatorial wind is thermally driven out; small scale and turbulent magnetic fields may be responsible for launching the plasma out of the disk via magnetic reconnections. The dusty torus and BLR in a RQQ are not shown.
- $\dot{m} \sim 0.03$: the thin disk is made of an inner and outer part; the inner disk extends to around ISCO. The two-phase ADAF is clumpy, so the jet produced via a mixture of the BP and BZ mechanisms is discontinuous. The dusty torus and BLR in a BL Lac are not shown.
- $\dot{m} < 0.01$: "Q" refers to the very low luminosity quiescent state that normally displays a hard power-law spectrum. The large scale magnetic fields rotating with the truncated thin disk and thick ADAF channel the continuous plasma to form collimated and continuous jets via the BP mechanism. There is neither dusty torus nor BLR in LLAGNs [179].

Fig. 40 Unification scheme of accretion-outflow connections of accreting BHs for different ranges of accretion rates, corresponding to different spectral states or different types of astrophysical systems. From very low to very high accretion rates in units of the Eddington rate $\dot{m}$, these states are: hard/quiescent state, hard/low state, thermal-dominated soft state, steep power-law state, slim disk, and NDAF disk; different types of AGNs with similar accretion-outflow structures are also labeled for comparison. The ubiquitous dusty tori and BLRs are absent in all BHXBs and microquasars. The lack of dusty tori can be easily understood since there is no dust supply in them. It is then plausible that the lack of BLRs is the consequence of no dusty tori, suggesting that a BLR may be formed out of the evaporated inner dusty torus by the anisotropic radiation of the accretion disk in an AGN [179].

decades on the study of BHXBs and microquasars, there are still many outstanding and unresolved issues, which can be pierced by two big pictures. One big picture is related to the astrophysics of BHXBs and microquasars, which is centered on understanding the accretion-outflow (wind or jet) connections at different accretion rates for different types of astrophysical systems involving BHs. The other big picture is related to the fundamental physics of BHXBs and microquasars, which is centered on identifying astrophysical BHs and testing theories of strong gravity. These two pictures are actually also entangled together, because a strong gravity theory, such as GR, is needed to describe the astrophysical aspects of these systems, and we need to understand the astro-

physics of BHXBs and microquasars before we can start to test any strong gravity theory [174].

Figure 39 shows the relation between the collimation-corrected gamma-ray luminosity and the kinetic power for AGNs and gamma-ray bursts (GRBs) [175]. For at least some of GRBs, a super-Eddington accreting compact stellar object, probably a BH with around $10M_{\odot}$, is believed to be responsible for powering the highly relativistic jets, which produces intense gamma-rays through violent collisions of blobs in the jets [176]. The two types of AGNs shown here, flat-spectrum radio quasars (FSRQs) and BL Lacs, have all been observed to have mildly relativistic jets. Their central engines are supermassive BHs with around $10^{7-9}M_{\odot}$ with accretion rates just below (for FSRQs) or far below (for BL Lacs) Eddington rate [177]. The good correlation over about 10 orders of magnitudes between these very different systems with very different accretion rates suggests that there must be some common mechanisms responsible for the accretion-outflow (wind/jet) connections for all accreting BHs [178].

Putting together all related phenomenologies and some theoretical modeling of BHXBs and microquasars discussed in this article, an unification scheme is illustrated in Fig. 40 with the major elements in the accretion-outflow connections in different types of astrophysical systems harboring both stellar mass BHs and supermassive BHs with accretion rates over several orders of magnitudes. The types of accreting stellar mass BHs include BHXBs and microquasars in different spectral states, as well as ultra-luminous X-ray sources (ULXs) (some of which are most likely ultra-Eddington accreting BHs [180]), and GRBs. The types of accreting supermassive mass BHs include low-luminosity AGNs (LLAGNs), BL Lac objects, normal radio quiet quasars (RQQs), FSRQs and broad-line-less luminous quasars (BL3Qs) [179] (I create the acronym "BL3Q" here just for fun).

This scheme is not a theoretical model, or even toy model yet. It, however, can be used as one possible chain to pierce many observed phenomenologies together, providing a possible frame work for further theoretical developments on accretion-outflow connections. Future observations will scrutinize this unification scheme and revise it inevitably. Of particular importance is the reliable determinations of the mass and spin of accreting BHs. The BH mass allows us to determine the accretion rate in units of Eddington rate, i.e., $\dot{m}$, which is a key parameter to the unification scheme of accretion-outflow connections. The BH spin is of course another key parameter, because it can determine the radiative efficiency of the disk and jet power in the BZ mechanism.

Once we have well determined BH parameters and a consistent and predictable theory describing the observed accretion-outflow connections, we are then ready to study the fundamental physics of BHs with BHXBs and microquasars, such as the properties of event horizon, space-time around Schwarzschild and Kerr BHs, BH spin energy (and mass) extraction. For example, both the broad iron line and CF fitting methods can be used to measure a BH's spin. However the two methods are equivalent only if the metric is accurately described with Kerr metric. Different spin measurements for a BH with the two different methods would invalidate Kerr metric, provided that we understand the accretion disk physics thoroughly. On the other hand, a correct metric is of course required to describe accurately the accretion flow around BHs. This is one example of the entanglement or interplay between astrophysics and fundamental physics of accreting BHs. The stake is high, but the job is difficult.

Acknowledgements I appreciate inputs from Profs. Lijun Gou, Weimin Gu, Lixin Li, Bifang Liu, Dingxiong Wang, Wenfei Yu, Feng Yuan, and Shu Zhang. The editors of this book are thanked for inviting me to write this article, as well as their patience, persistency, proof reading it, and offering comments and suggestions to improve it in the end. This work was partially supported with funding the 973 Program of China under grant 2009CB824800, by the National Natural Science Foundation of China under grant Nos. 11133002 and 10725313, and the Qianren start-up grant 292012312D1117210.

References

1. R. Fender and T. Belloni, Science, 2012, 337(6094): 540
2. R. A. Remillard and J. E. McClintock, Annu. Rev. Astron. Astrophys., 2006, 44(1): 49
3. C. Done, Observational characteristics of accretion onto black holes, To appear in XXI Canary Islands Winter School of Astrophysics, edited by T. Shahbaz, CUP, 2010: 56
4. C. Done, M. Gierliski, and A. Kubota, Astron. Astrophys. Rev., 2007, 15(1): 1
5. S. N. Zhang, in: Astronomy Revolution: 400 Years of Exploring the Cosmos, edited by S. N. Zhang, D. G. York, and O. Gingerich, chapter Astrophysics, Taylor & Francis Group LLC/CRC Press, 2011: 23
6. Ya. B. Zel'dovich and I. D. Novikov, Sov. Phys. Usp., 1966, 8(4): 522
7. Ya. B. Zel'dovich and I. D. Novikov, Sov. Phys. Usp., 1965, 7(6): 763
8. B. L. Webster and P. Murdin, Nature, 1972, 235(5332): 37
9. I. F. Mirabel, L. F. Rodríguez, B. Cordier, J. Paul, and F. Lebrun, Nature, 1992, 358(6383): 215
10. I. F. Mirabel and L. F. Rodríguez, Nature, 1994, 371(6492): 46
11. S. N. Zhang, C. A. Wilson, B. A. Harmon, G. J. Fishman, W. S. Paciesas, and M. Scott, IAUC 6046: X-Ray N IN Sco; 1994W. IAU Circ., 6046(1), 1994.

12. S. J. Tingay, D. L. Jauncey, R. A. Preston, J. E. Reynolds, et al., Nature, 1995, 374(6518): 141
13. B. A. Harmon, C. A. Wilson, S. N. Zhang, W. S. Paciesas, G. J. Fishman, R. M. Hjellming, M. P. Rupen, D. M. Scott, M. S. Briggs, and B. C. Rubin, Nature, 1995, 374(6524): 703
14. I. F. Mirabel and L. F. Rodríguez, Annu. Rev. Astron. Astrophys., 1999, 37(1): 409
15. R. Fender, K. Wu, H. Johnston, T. Tzioumis, P. Jonker, R. Spencer, and M. van der Klis, Nature, 2004, 427(6971): 222
16. J. F. Hao and S. N. Zhang, Astrophys. J., 2009, 702(2): 1648
17. D. A. Kniffen, W. C. K. Alberts, D. L. Bertsch, B. L. Dingus, et al., Astrophys. J., 1997, 486(1): 126
18. J. M. Paredes, J. Mart, and M. Massi, Science, 2000, 288(5475): 2340
19. F. Aharonian, A. G. Akhperjanian, K. M. Aye, A. R. Bazer-Bachi, et al., Science, 2005, 309(5735): 746
20. F. Aharonian, Science, 2005, 307(5717): 1938
21. I. F. Mirabel, Astrophys. Space Sci., 2007, 309(1–4): 267
22. W. Cui, Research in Astronomy and Astrophysics, 2009, 9(8): 841
23. G. E. Romero, Proceedings of the International Astronomical Union, 2010, 5(H15): 126
24. J. Li, D. F. Torres, S. Zhang, D. Hadasch, N. Rea, G. A. Caliandro, Y. P. Chen, and J. M. Wang, Astrophys. J., 2012, 744(1): L13
25. K. S. Thorne, Science, 2012, 337(6094): 536
26. E. Witten, Science, 2012, 337(6094): 538
27. M. Volonteri, Science, 2012, 337(6094): 544
28. T. M. Belloni, S. E. Motta, and T. M. Darias, Bulletin of the Astronmical Society of India, 2011, 39(3): 409
29. J. N. Zhou, Q. Z. Liu, Y. P. Chen, J. Li, J. L. Qu, S. Zhang, H. Q. Gao, and Z. Zhang, The last three outbursts of H1743-322 observed by RXTE in its latest service phase, Monthly Notice of the Royal Astronomical Society, 2013
30. A. G. Cantrell, C. D. Bailyn, J. A. Orosz, J. E. McClintock, R. A. Remillard, C. S. Froning, J. Neilsen, D. M. Gelino, and L. J. Gou, Astrophys. J., 2010, 710(2): 1127
31. L. J. Gou, J. E. McClintock, J. F. Steiner, R. Narayan, A. G. Cantrell, C. D. Bailyn, and J. A. Orosz, Astrophys. J., 2010, 718(2): L122
32. R. Shafee, J. E. McClintock, R. Narayan, and S. W. Davis, Astrophys. J., 2006, 636(2): L113
33. J. F. Steiner, R. C. Reis, J. E. McClintock, R. Narayan, R. A. Remillard, J. A. Orosz, L. J. Gou, A. C. Fabian, and M. A. P. Torres, Mon. Not. R. Astron. Soc., 2011, 416(2): 941
34. J. F. Steiner, J. E. McClintock, and M. J. Reid, Astrophys. J., 2012, 745(1): L7
35. J. E. McClintock, R. Shafee, R. Narayan, R. A. Remillard, S. W. Davis, and L. X. Li, Astrophys. J., 2006, 652(1): 518
36. J. A. Orosz, J. E. McClintock, J. P. Aufdenberg, R. A. Remillard, M. J. Reid, R. Narayan, and L. J. Gou, Astrophys. J., 2011, 742(2): 84
37. L. J. Gou, J. E. McClintock, M. J. Reid, J. A. Orosz, J. F. Steiner, R. Narayan, J. G. Xiang, R. A. Remillard, K. A. Arnaud, and S. W. Davis, Astrophys. J., 2011, 742(2): 85
38. S. W. Davis, C. Done, and O. M. Blaes, Astrophys. J., 2006, 647(1): 525
39. J. A. Orosz, D. Steeghs, J. E. McClintock, M. A. P. Torres, I. Bochkov, L. J. Gou, R. Narayan, M. Blaschak, A. M. Levine, R. A. Remillard, C. D. Bailyn, M. M. Dwyer, and M. Buxton, Astrophys. J., 2009, 697(1): 573
40. L. J. Gou, J. E. McClintock, Jifeng Liu, R. Narayan, J. F. Steiner, R. A. Remillard, J. A. Orosz, S. W. Davis, K. Ebisawa, and E. M. Schlegel, Astrophys. J., 2009, 701(2): 1076
41. J. F. Steiner, R. C. Reis, A. C. Fabian, R. A. Remillard, J. E. McClintock, L. J. Gou, R. Cooke, L. W. Brenneman, and J. S. Sanders, Mon. Not. R. Astron. Soc., 2012, 427(3): 2552
42. A. H. Prestwich, R. Kilgard, P. A. Crowther, S. Carpano, A. M. T. Pollock, A. Zezas, S. H. Saar, T. P. Roberts, and M. J. Ward, Astrophys. J., 2007, 669(1): L21
43. J. M. Silverman and A. V. Filippenko, Astrophys. J., 2008, 678(1): L17
44. P. A. Crowther, R. Barnard, S. Carpano, J. S. Clark, V. S. Dhillon, and A. M. T. Pollock, Mon. Not. R. Astron. Soc. Lett., 2010, 403(1): L41
45. J. A. Orosz, J. E. McClintock, R. Narayan, C. D. Bailyn, J. D. Hartman, L. Macri, J. F. Liu, W. Pietsch, R. A. Remillard, A. Shporer, and T. Mazeh, Nature, 2007, 449(7164): 872
46. J. F. Liu, J. E. McClintock, R. Narayan, S. W. Davis, and J. A. Orosz, Astrophys. J., 2010, 719(1): L109
47. S. N. Zhang, W. Cui, and W. Chen, Astrophys. J., 1997, 482(2): L155
48. J. E. McClintock, R. Narayan, S. W. Davis, L. J. Gou, A. Kulkarni, J. A. Orosz, R. F. Penna, R. A. Remillard, and J. F. Steiner, Class. Quantum Grav., 2011, 28(11): 114009
49. J. P. Lasota, New Astron. Rev., 2001, 45(7): 1993
50. J. P. Lasota, Mem. Soc. Astron. Ital., 2012, 83: 469
51. N. I. Shakura and R. A. Sunyaev, Astron. Astrophys., 1973, 24: 337
52. D. N. Page and K. S. Thorne, Astrophys. J., 1974, 191: 499
53. J. Neilsen and J. C. Lee, Nature, 2009, 458(7237): 481
54. G. Ponti, R. P. Fender, M. C. Begelman, R. J. H. Dunn, J. Neilsen, and M. Coriat, Mon. Not. R. Astron. Soc. Lett., 2012, 422(1): L11
55. M. A. Abramowicz and W. Kluźniak, Astron. Astrophys., 2001, 374(3): L19
56. G. Török, M. A. Abramowicz, W. Kluźniak, and Z. Stuchlík, Astron. Astrophys., 2005, 436(1): 1
57. C. Y. Huang, Z. M. Gan, J. Z. Wang, and D. X. Wang, Mon. Not. R. Astron. Soc., 2010, 403(4): 1978
58. M. Kolehmainen and C. Done, Mon. Not. R. Astron. Soc., 2010, 406(4): 2206
59. R. Narayan and I. Yi, Astrophys. J., 1995, 452: 710
60. B. F. Liu, W. Yuan, F. Meyer, E. Meyer-Hofmeister, and G. Z. Xie, Astrophys. J., 1999, 527(1): L17
61. J. M. Miller, Annu. Rev. Astron. Astrophys., 2007, 45(1): 441
62. A. R. King, U. Kolb, and E. Szuszkiewicz, Astrophys. J., 1997, 488(1): 89
63. D. Altamirano, T. Belloni, M. Linares, M. van der Klis, R. Wijnands, P. A. Curran, M. Kalamkar, H. Stiele, S. Motta, T. M. Darias, P. Casella, and H. Krimm, Astrophys. J., 2011, 742(2): L17
64. S. S. Weng and S. N. Zhang, Astrophys. J., 2011, 739(1): 42
65. Y. S. Yao, S. N. Zhang, X. L. Zhang, Y. X. Feng, and C. R. Robinson, Astrophys. J., 2005, 619(1): 446

66. S. N. Zhang, Highlights of Astronomy, 2007, 14: 14
67. L. Wang, C. Fang, and Y. Y. Liu, Astrophys. Space Sci., 2008, 318(1-2): 79
68. J. Biteau and B. Giebels, Astron. Astrophys., 2012, 548: A123
69. J. M. Bardeen, Nature, 1970, 226(5240): 64
70. K. S. Thorne, Astrophys. J., 1974, 191: 507
71. A. R. King and U. Kolb, Mon. Not. R. Astron. Soc., 1999, 305(3): 654
72. R. Narayan and J. E. McClintock, Mon. Not. R. Astron. Soc. Lett., 2012, 419(1): L69
73. J. F. Steiner, J. E. McClintock, and R. Narayan, Astrophys. J., 2013, 762(2): 104
74. R. P. Fender, E. Gallo, and D. Russell, Mon. Not. R. Astron. Soc., 2010, 406: 1425, arXiv: 1003.5516 [astro-ph.HE]
75. R. D. Blandford and D. G. Payne, Mon. Not. R. Astron. Soc., 1982, 199: 883
76. R. D. Blandford and R. L. Znajek, Mon. Not. R. Astron. Soc., 1977, 179: 433
77. L. Xue, A. Sdowski, M. A. Abramowicz, and J.-F. Lu, Astrophys. J. Suppl. Ser., 2011, 195(1): 7
78. J. M. Bardeen, W. H. Press, and S. A. Teukolsky, Astrophys. J., 1972, 178: 347
79. S. N. Zhang, K. Ebisawa, R. Sunyaev, Y. Ueda, B. A. Harmon, S. Sazonov, G. J. Fishman, H. Inoue, W. S. Paciesas, and T. Takahash, Astrophys. J., 1997, 479(1): 381
80. J. A. Orosz and C. D. Bailyn, Astrophys. J., 1997, 477(2): 876
81. L.-X. Li, E. R. Zimmerman, R. Narayan, and J. E. McClintock, Astrophys. J. Suppl., 2005, 157(2): 335
82. S. W. Davis and I. Hubeny, Astrophys. J. Suppl., 2006, 164(2): 530
83. J. E. McClintock and R. A. Remillard, Measuring the Spins of Stellar-Mass Black Holes, Astro2010 Science White Paper, February 2009
84. R. F. Penna, J. C. McKinney, R. Narayan, A. Tchekhovskoy, R. Shafee, and J. E. McClintock, Mon. Not. R. Astron. Soc., 2010, 408(2): 752
85. A. K. Kulkarni, R. F. Penna, R. V. Shcherbakov, J. F. Steiner, R. Narayan, A. Sdowski, Y. C. Zhu, J. E. McClintock, S. W. Davis, and J. C. McKinney, Mon. Not. R. Astron. Soc., 2011, 414(2): 1183
86. Y. C. Zhu, S. W. Davis, R. Narayan, A. K. Kulkarni, R. F. Penna, and J. E. McClintock, Mon. Not. R. Astron. Soc., 2012, 424(4): 2504
87. J. F. Steiner, J. E. McClintock, R. A. Remillard, R. Narayan, and L. J. Gou, Astrophys. J., 2009, 701(2): L83
88. J. F. Steiner, J. E. McClintock, R. A. Remillard, L. J. Gou, S. Yamada, and R. Narayan, Astrophys. J., 2010, 718(2): L117
89. D. C. Lin, R. A. Remillard, and J. Homan, Astrophys. J., 2009, 696(2): 1257
90. S. S. Weng, S. N. Zhang, and H. H. Zhao, Astrophys. J., 2013 (submitted)
91. W. M. Gu, Astrophys. J., 2012, 753(2): 118
92. X. Chen, S. N. Zhang, and G. Q. Ding, Astrophys. J., 2006, 650(1): 299
93. F. Yuan, W. Cui, and R. Narayan, Astrophys. J., 2005, 620(2): 905
94. S. N. Zhang, W. Cui, B. A. Harmon, W. S. Paciesas, R. E. Remillard, and J. van Paradijs, Astrophys. J., 1997, 477(2): L95
95. Q. J. Yu and S. Tremaine, Mon. Not. R. Astron. Soc., 2002, 335(4): 965
96. T. W. Wong, F. Valsecchi, T. Fragos, and V. Kalogera, Astrophys. J., 2012, 747(2): 111
97. J. F. Steiner, R. Narayan, J. E. McClintock, and K. Ebisawa, Publ. Astron. Soc. Pac., 2009, 121(885): 1279
98. A. G. Cantrell, C. D. Bailyn, J. E. McClintock, and J. A. Orosz, Astrophys. J., 2008, 673(2): L159
99. L. Kreidberg, C. D. Bailyn, W. M. Farr, and V. Kalogera, Astrophys. J., 2012, 757(1): 36
100. F. van der Hooft, F. Alberts, and J. van Paradijs, Astron. Astrophys., 1998, 550: 538
101. S. N. Phillips, T. Shahbaz, and Ph. Podsiadlowski, Mon. Not. R. Astron. Soc., 1999, 304(4): 839
102. T. Shahbaz, F. van der Hooft, J. Casares, P. A. Charles, and J. van Paradijs, Mon. Not. R. Astron. Soc., 1999, 306(1): 89
103. J. Greene, C. D. Bailyn, and J. A. Orosz, Astrophys. J., 2001, 554(2): 1290
104. M. E. Beer and P. Podsiadlowski, Mon. Not. R. Astron. Soc., 2002, 331(2): 351
105. T. Shahbaz, Mon. Not. R. Astron. Soc., 2003, 339(4): 1031
106. J. M. Bardeen and J. A. Petterson, Astrophys. J., 1975, 195: L65
107. R. M. Hjellming and M. P. Rupen, Nature, 1995, 375(6531): 464
108. C. Foellmi, E. Depagne, T. H. Dall, and I. F. Mirabel, Astron. Astrophys., 2006, 457(1): 249
109. C. Foellmi, New Astron., 2009, 14(8): 674
110. D. Steeghs and J. Casares, Astrophys. J., 2002, 568(1): 273
111. C. A. Haswell and A. W. Shafter, Astrophys. J., 1990, 359: L47
112. J. A. Orosz, C. D. Bailyn, R. A. Remillard, J. E. McClintock, and C. B. Foltz, Astrophys. J., 1994, 436: 848
113. R. Soria, D. T. Wickramasinghe, R. W. Hunstead, and K. Wu, Astrophys. J., 1998, 495(2): L95
114. S. N. Zhang, J. Y. Liao, and Y. S. Yao, Mon. Not. R. Astron. Soc., 2012, 421(4): 3550
115. J. M. Miller, J. Raymond, A. Fabian, D. Steeghs, J. Homan, C. Reynolds, M. van der Klis, and R. Wijnands, Nature, 2006, 441(7096): 953
116. P. A. Connors and R. F. Stark, Nature, 1977, 269(5624): 128
117. P. A. Connors, R. F. Stark, and T. Piran, Astrophys. J., 1980, 235: 224
118. L.-X. Li, R. Narayan, and J. E. McClintock, Astrophys. J., 2009, 691(1): 847
119. J. D. Schnittman and J. H. Krolik, Astrophys. J., 2009, 701(2): 1175
120. S. Chandrasekhar, Radiative Transfer, New York: Dover, 1960.
121. J. M. Miller, C. S. Reynolds, A. C. Fabian, E. M. Cackett, G. Miniutti, J. Raymond, D. Steeghs, R. Reis, and J. Homan, Astrophys. J., 2008, 679(2): L113

122. J. M. Miller, C. S. Reynolds, A. C. Fabian, G. Miniutti, and L. C. Gallo, Astrophys. J., 2009, 697(1): 900
123. R. C. Reis, A. C. Fabian, R. R. Ross, and J. M. Miller, Mon. Not. R. Astron. Soc., 2009, 395(3): 1257
124. Z. X. Ling, S. N. Zhang, J. G. Xiang, and S. C. Tang, Astrophys. J., 2009, 690(1): 224
125. Z. X. Ling, S. N. Zhang, and S. C. Tang, Astrophys. J., 2009, 695(2): 1111
126. M. J. Reid, J. E. McClintock, R. Narayan, Lijun Gou, R. A. Remillard, and J. A. Orosz, Astrophys. J., 2011, 742(2): 83
127. B. Czerny, K. Hryniewicz, M. Nikoajuk, and A. Sadowski, Mon. Not. R. Astron. Soc., 2011, 415(3): 2942
128. M. Kishimoto, R. Antonucci, O. Blaes, A. Lawrence, C. Boisson, M. Albrecht, and C. Leipski, Nature, 2008, 454(7203): 492
129. R. Y. Hu and S. N. Zhang, Mon. Not. R. Astron. Soc., 2012, 426(4): 2847
130. H. Zhang, F. Yuan, and S. Chaty, Astrophys. J., 2010, 717(2): 929
131. F. Yuan, Z. Yu, and L. C. Ho, Astrophys. J., 2009, 703(1): 1034
132. F. Yuan and W. Cui, Astrophys. J., 2005, 629(1): 408
133. F. Yuan, Astrophys. J., 2003, 594(2): L99
134. F. Yuan, A. A. Zdziarski, Y. Q. Xue, and X. B. Wu, Astrophys. J., 2007, 659(1): 541
135. F. Meyer and B. F. Liu, Astron. Astrophys., 2000, 361: 175
136. F. Meyer and B. F. Liu, Astron. Astrophys., 2000, 354: L67
137. B. F. Liu, S. Mineshige, F. Meyer, E. Meyer-Hofmeister, and T. Kawaguchi, Astrophys. J., 2002, 575(1): 117
138. B. F. Liu, R. E. Taam, E. Meyer-Hofmeister, and F. Meyer, Astrophys. J., 2007, 671(1): 695
139. B. F. Liu, C. Done, and R. E. Taam, Astrophys. J., 2011, 726(1): 10
140. B. F. Liu, F. Meyer, and E. Meyer-Hofmeister, Astron. Astrophys., 2006, 454(1): L9
141. F. Meyer, B. F. Liu, and E. Meyer-Hofmeister, Astron. Astrophys., 2007, 463(1): 1
142. R. E. Taam, B. F. Liu, F. Meyer, and E. Meyer-Hofmeister, Astrophys. J., 2008, 688(1): 527
143. E. L. Qiao and B. F. Liu, Publ. Astron. Soc. Jpn., 2009, 61(2): 403
144. E. L. Qiao and B. F. Liu, Astrophys. J., 2012, 744(2): 145
145. B. F. Liu, F. Meyer, and E. Meyer-Hofmeister, Astron. Astrophys., 2005, 442(2): 555
146. E. Meyer-Hofmeister, B. F. Liu, and F. Meyer, Astron. Astrophys., 2005, 432(1): 181
147. E. Meyer-Hofmeister, B. F. Liu, and F. Meyer, Astron. Astrophys., 2009, 508(1): 329
148. J. M. Wang, C. Cheng, and Y. R. Li, Astrophys. J., 2012, 748(2): 147
149. S. N. Zhang, B. A. Harmon, W. S. Paciesas, G. J. Fishman, J. E. Grindlay, D. Barret, M. Tavani, P. Kaaret, P. Bloser, E. Ford, and L. Titarchuk, Astron. Astrophys. Suppl., 1996, 120: 279
150. Y. P. Chen, S. Zhang, S. N. Zhang, J. Li, and J. M. Wang, Astrophys. J., 2012, 752(2): L34
151. S. N. Zhang, Science, 2000, 287(5456): 1239
152. F. Yuan and J. Lin, Mon. Not. R. Astron. Soc., 2009, 395(4): 2183
153. B. Czerny, M. Nikołajuk, A. Różańska, A. M. Dumont, Z. Loska, and P. T. Życki, Astron. Astrophys., 2003, 412(2): 317
154. Y. L. Ai, W. Yuan, H. Y. Zhou, T. G. Wang, and S. H. Zhang, Astrophys. J., 2011, 727(1): 31
155. C. Done, S. W. Davis, C. Jin, O. Blaes, and M. Ward, Mon. Not. R. Astron. Soc., 2012, 420(3): 1848
156. S. Nayakshin and F. Melia, Astrophys. J., 1997, 490(1): L13
157. S. Nayakshin and J. B. Dove, Astrophys. J., 2001, 560(2): 885
158. W. F. Yu, M. van der Klis, and R. Fender, Astrophys. J., 2004, 611(2): L121
159. W. F. Yu, F. K. Lamb, R. Fender, and M. van der Klis, Astrophys. J., 2007, 663(2): 1309
160. W. F. Yu and J. Dolence, Astrophys. J., 2007, 667(2): 1043
161. W. F. Yu and Z. Yan, Astrophys. J., 2009, 701(2): 1940
162. J. Tang, W. F. Yu, and Z. Yan, Research in Astronomy and Astrophysics, 2011, 11(4): 434
163. A. P. Lightman and D. M. Eardley, Astrophys. J., 1974, 187: L1
164. N. I. Shakura and R. A. Sunyaev, Mon. Not. R. Astron. Soc., 1976, 175: 613
165. T. Piran, Astrophys. J., 1978, 221: 652
166. M. Gierlinski and C. Done, Mon. Not. R. Astron. Soc., 2004, 347(3): 885
167. A. A. Zdziarski and M. Gierliski, Prog. Theor. Phys. Suppl., 2004, 155: 99
168. S. Hirose, J. H. Krolik, and O. Blaes, Astrophys. J., 2009, 691(1): 16
169. S. M. Zheng, F. Yuan, W. M. Gu, and J. F. Lu, Astrophys. J., 2011, 732(1): 52
170. T. Belloni, M. M é ndez, A. R. King, M. van der Klis, and J. van Paradijs, Astrophys. J., 1997, 479(2): L145
171. S. Nayakshin, S. Rappaport, and F. Melia, Astrophys. J., 2000, 535(2): 798
172. A. Janiuk, B. Czerny, and A. Siemiginowska, Astrophys. J., 2002, 576(2): 908
173. D. B. Lin, W. M. Gu, and J. F. Lu, Mon. Not. R. Astron. Soc., 2011, 415(3): 2319
174. M. A. Abramowicz and P. C. Fragile, Living Reviews in Relativity, 2013, 16(1): 1
175. R. S. Nemmen, M. Georganopoulos, S. Guiriec, E. T. Meyer, N. Gehrels, and R. M. Sambruna, Science, 2012, 338(6113): 1445
176. B. Zhang, Chin. J. Astron. Astrophys., 2007, 7(1): 1
177. J. Zhang, E. W. Liang, S. N. Zhang, and J. M. Bai, Astrophys. J., 2012, 752(2): 157
178. S. N. Zhang, Proceedings of the International Astronomical Union, 2007, 2(14): 14
179. Y. Liu and S. N. Zhang, Astrophys. J., 2011, 728(2): L44
180. H. Feng and R. Soria, New Astron. Rev., 2011, 55(5–6): 166